Advancements in the use of Auger electrons in science and medicine during the period 2015–2019

ROGER W. HOWELL

Division of Radiation Research, Department of Radiology, New Jersey Medical School, Rutgers University, Newark, NJ 07103

Abstract

Purpose: Auger electrons can be highly radiotoxic when they are used to irradiate specific molecular sites continues. This has spurred basic-science investigations of their radiobiological effects and clinical investigations of their potential for therapy. Focused symposia on the biophysical aspects of Auger processes have been held quadrennially. This 9th International Symposium on Physical, Molecular, Cellular, and Medical Aspects of Auger Processes at Oxford University brought together scientists from many different fields to review past findings, discuss the latest studies, and plot the future work to be done. This review article examines the research in this field that was published during the years 2015–2019 which corresponds to the period since the last meeting in Japan. In addition, this article points to future work yet to be done.

Conclusions: There have been a plethora of advancements in our understanding of Auger processes. These advancements range from basic atomic and molecular physics to new ways to implement Auger electron emitters in radiopharmaceutical therapy. The highly localized doses of radiation that are deposited within a 10 nm of the decay site make them precision tools for discovery across the physical, chemical, biological and medical sciences.

Introduction

There is a very large body of literature that has developed over the 100 years that have elapsed since the discovery of Auger electrons by Pierre Auger. The purpose of this article is to primarily review the literature that was published during the period 2015–2019, although some citations to earlier work are included to make specific points. This review begins with a brief description of the physical basis of Auger processes and then goes on to describe the published research and its implications.

The removal of an inner shell electron from an atom leaves the atom in an excited state. Atomic relaxation to the ground state occurs via radiative and non-radiative processes within the atom containing the original vacancy, and via processes that take place in

neighboring atoms. Radiative processes are those that emit photons such as characteristic x-rays. Non-radiative processes emit Auger electrons, Coster-Kronig (CK) electrons, and super-CK electrons. These categories of electrons, often collectively referred to simply as Auger electrons, are characterized by the shells and subshells involved with the transition. Radiative processes dominate K-shell transitions, whereas non-radiative processes dominate when the vacancy is in the L-shell and above. Nevertheless, the vacancy is filled rapidly which leads to the creation new vacancies in higher subshells forming a cascade of atomic transitions that emit a shower of low energy Auger electrons and characteristic x-rays.

While it is straightforward to describe Auger processes in a single atom, additional deexcitation processes are possible when an inner atomic vacancy is created within atoms comprising a molecule. Cederbaum (Cederbaum et al. 1997) discovered interatomic coulombic decay (ICD), an atomic de-excitation process wherein a vacancy in the inner-*valence* region of an atom (~20–80 eV) can lead to the ejection of a valence electron from a *neighboring* atom. ICD has a substantial effect on Auger spectra that arise when vacancies are created in iodine atoms in molecules (Pernpointner and Knecht 2005; Pernpointner et al. 2006). Analogous to resonant Auger decay, there is yet another mechanism called resonant ICD (Barth et al. 2005). Thus, there are competing mechanisms in the relaxation of molecular electronic states that include ICD processes and Auger processes. The ICD electrons produced during these relaxation processes affect the radiation spectra produced (Figure 1).

Atomic vacancies that lead to Auger and ICD processes are created by several mechanisms. One mechanism that creates an inner atomic shell vacancy is the photoelectric effect. The Auger electrons that are emitted following the photoelectric effect were observed by Pierre Auger when he irradiated a cloud chamber with x-rays (Auger 1923). Radionuclides undergoing internal conversion (IC) transitions also create inner atomic shell vacancies, as do radionuclides that decay by electron capture (EC). The shower of low energy electrons that follow was seen by Meitner when she was conducting experiments on radioactive decay (Meitner 1923). The stochastic nature of the atomic and molecular electronic relaxation process results in different yields and energies of electrons for each initial vacancy created. Most of these electrons have very low energies (~ 20 eV to 500 eV) which have extremely short ranges in water (~ 1–10 nm). Biological molecules near the Auger cascade are impacted by the direct effects of electron irradiation was well as indirect effects caused by radical species that are produced during the radiolysis of water by these electrons (Figure 2) (Wright et al. 1990). Other physical mechanisms such as Coulomb explosion, caused by extremely rapid charge neutralization of highly ionized atoms, can cause damage to the molecule in which electronic vacancies are created (Pomplun and Sutmann 2004).

The radiobiological implications of Auger processes are of importance to many fields such as radiation therapy, diagnostic radiology, radiation safety, and radiobiology. Radionuclides that decay by EC and IC are used in nuclear medicine and in basic research laboratories. These include ^{55}Fe, ^{67}Ga, ^{77}Br, ^{99m}Tc, ^{111}In, ^{123}I, ^{125}I, ^{201}Tl and others. These radionuclides attracted significant attention when several laboratories observed unexpectedly high radiotoxicity when they decay within DNA (Ertl et al. 1970; Hofer and Hughes 1971; Bradley et al. 1975; Feinendegen 1975). When localized in DNA, Auger electron emitters

have been shown to be more radiotoxic than the alpha particle emitter ^{210}Po (Howell et al. 1990; Rao et al. 1990). The biological effects of Auger electron emitters are caused by a variety of factors, the determinant of the principal factor being the location of the decay site. High-LET type effects, manifested by exponential clonogenic cell survival curves and high values of relative biological effectiveness (RBE), have been observed when the radionuclide is localized within the DNA, however the radiation-induced damage to the DNA is caused largely by the indirect action of radical species (Narra et al. 1992; Harapanhalli et al. 1994; Goddu et al. 1996; Walicka M. A. et al. 1998a, 1998b; Bishayee et al. 2000; Walicka M.A. et al. 2000). Low-LET type effects, manifested by a shouldered clonogenic cell survival curve, and low RBE are observed when the radionuclide is localized in the cytoplasm. Localization of the Auger electron emitter on the cell membrane imparts detrimental effects between those observed for DNA and cytoplasmic localizations (Pouget et al. 2008). Radiation-induced bystander effects also play a significant role in the radiotoxicity of Auger electrons emitters (Howell and Bishayee 2002; Xue et al. 2002; Akudugu et al. 2012). The latter may play a major role in the clinical implementation of Auger electron emitters for radiopharmaceutical therapy (Prise and O'Sullivan 2009).

Over the years, numerous reviews have been published on the biological effects of Auger electron emitters (Sastry and Rao 1984; Sastry KSR 1992; Kassis 2004; Nikjoo et al. 2006; Howell 2008; Martin and Feinendegen 2016). The renewed interest in their potential for therapeutic applications prompted a host of additional reviews during the period 2015–2019 (Gudkov et al. 2015; Guerra Liberal et al. 2016; Liko et al. 2016; Aghevlian et al. 2017; DeJesus 2017; Gill et al. 2017; Muller C et al. 2017; Rezaee et al. 2017; Widel 2017; Yokoya and Ito 2017; Bavelaar et al. 2018; Boros and Holland 2018; Martins et al. 2018; Muller C et al. 2018; Sobolev 2018; Tsai and Wu 2018; Boros and Packard 2019; Gill and Vallis 2019; Ku et al. 2019). These are recommended reading for those interested in learning about, or keeping up, with this field of study.

There has been a series of international meetings on the biological effects of Auger electron emitters, beginning with the 1975 meeting in Jülich, Germany. This meeting was followed by regular meetings on a quadrennial basis:

1st	1987	Charney Basset, UK (Baverstock and Charton 1988),
2nd	1991	Amherst, USA (Adelstein 1992; Howell et al. 1992),
3rd	1995	Lund, Sweden (Hofer 1996),
4th	1999	Lund, Sweden (Hofer 2000),
5th	2003	Melbourne, AUS (Kassis 2004),
6th	2007	Boston, USA (Howell 2008),
7th	2011	Jülich, Germany (Yasui 2012),
8th	2015	Kyoto, Japan (Martin and Feinendegen 2016),
9th	2019	Oxford, UK (this review).

A proceedings of each meeting has been published, including reviews of the status of the field, as referenced above. The present manuscript arises from the 2019 meeting at

Worcester College, University of Oxford and it reviews articles concerning biophysical aspects of Auger processes that were published from 2015 to 2019. In addition, the Oxford location allowed us to reflect on the contributions of pioneers in biophysical aspects of Auger processes who were at the 1987 meeting near Oxford, namely the late David Charlton (Humm and Nikjoo 2013) and Kandula Sastry (Howell and Rao 2002). David Charlton, together with Keith Baverstock, organized the 1987 meeting at Charney Manor, not far from the present meeting at Oxford. No one thought to bring a pointer (there were no laser pointers then) so David plucked a stick from the woods and a pointer was born. This relic has been passed formally from one meeting organizer to the next. The stick traveled around the world many times and then back to Oxford, the "home" of Harry Potter, where the stick was magically transformed into the *Auger Wand* by the meeting attendees during the opening lecture of the 2019 meeting. We look forward to seeing its magic in the form of new science at the 2023 meeting.

Review of the literature 2015–2019

Physics and Chemistry of Auger cascades

Although radiopharmaceutical therapy with Auger electron emitters has not gained significant traction in the clinic, the discovery of Auger-induced bystander effects by both DNA-incorporated and cell-membrane localized Auger electron emitters has reinvigorated interest in them for radiopharmaceutical therapy (Prise and O'Sullivan 2009; Pouget et al. 2018). Accordingly, it is important to have more accurate values of the yields and energies of Auger electrons emitted by radionuclides for use in dose-response analyses and modeling. Theoretical calculations have largely been the source of these data. A key component of these simulations is the conversion electron yield. Alotiby et al. measured the relative yields of Auger and conversion electrons emitted by ^{125}I on a silver surface (Alotiby et al. 2018). The resulting Auger electron yields that were determined from their experimental measurements differ by 20% from theoretical values published in the Evaluated Atomic Data Library (EADL) underestimate.

Lee et al. benchmarked a theoretical Monte Carlo model to simulate atomic relaxation processes and the corresponding Auger electron yields and energies against data in the literature (Lee BQ et al. 2016). They used the Evaluated Nuclear Structure Data Files (ENSDF) as input data. The initial vacancy distributions following EC and IC were determined using Schofield's algorithm. Atomic transition probabilities were taken from the EADL, whereas transition energies were calculated using relativistic Dirac-Fock methods. The average yields and energies of the radiations emitted by ^{123}I, ^{124}I, and ^{125}I were compared with published values (Pomplun et al. 1987; Howell 1992). Most of the results agreed the published data, with the exception of the electrons arising from the outer-shell Coster-Kronig and super Coster-Kronig transitions. Comparisons with the spectra in the MIRD Radionuclide Data and Decay Scheme Monograph would have been helpful (Eckerman and Endo 2008).

Pomplun conducted additional validations of his Monte Carlo code that simulates the shower of Auger electrons by comparing his theoretical results with experimental K-shell transition data for ^{55}Fe, ^{111}In and ^{125}I (Pomplun 2016). Transition probabilities for singly ionized

atoms were used along with and Auger electron energies were calculated with a Dirac–Fock program. The author felt that the timescale for charge transfer from the environment to the valence shells during the cascade was too long was electrons were not supplemented during the cascade. His K-shell results were in good agreement with the experimental data. The author noted that these simulations do not account for intermolecular Coulombic decay and attosecond-scale intermolecular electron transfer processes under investigation by others as described in this review article.

As pointed about above, the spectrum of Auger electrons emitted and their subsequent interaction with intracellular molecules such as water and DNA, are of importance to biological processes. These data, essential for theoretical simulations, have been the subject of recent atomic physics experiments. The experimental studies that are described below constitute a review of the developments in this scientific field.

Much can be learned about Auger electron spectra from the molecular photophysical processes that can be followed by measuring the energy of ejected electrons and scattered X-rays. Bennett et al. have derived a method to analyze time-resolved Auger-electron spectroscopy (AES), photoelectron spectroscopy (TRPES), and off-resonant X-ray scattering (OXS) (Bennett et al. 2015). In these types of experiments, the electronic and nuclear dynamics of nonstationary states are monitored. Electron spectroscopies depend on many variables such as valence, core, and continuum electronic states, nuclear degrees of freedom, and fluctuations that arise due to coupling to the environment. To further understand this, they created a theoretical model that describes the time-resolved electron and photon scattering spectroscopies that arise from molecules that are excited to nonstationary states. This approach may be useful for calculating Auger and CK transition rates and energies that change continuously as Auger cascades unfold. This has been a topic of considerable importance in theoretical predictions of Auger spectra that can arise from the decay of a given Auger electron emitter (Charlton and Booz 1981; Howell 1992; Pomplun 2000, 2016).

Other studies have also been conducted that relate to transition rates for Auger processes. Bizau et al. studied the $4d \rightarrow nf$ ($n \frac{1}{4}$ 4; 5) resonances in Auger decay of multiply ionized Xe^{5+} ions (Bizau et al. 2016). Using coincidence counting techniques, they detected Auger electrons and the resulting Xe^{6+} ions. The $5s5p$ satellite lines were observed to be up to 4x stronger than the $5s^2$ main lines. This unexpected behavior in experiments was checked with multiconfiguration Dirac-Fock calculations and good agreement was observed. The experimental approach they used is a stringent test for theoretical models of Auger transition rates for multiply ionized gaseous atoms.

Synchrotrons offer the ability to tune photons to selectively excite atoms in molecules. Bolognesi et al. used synchrotron radiation tuned to excite and ionize 2-nitroimidazole at the C, N, and O K-edges (Bolognesi et al. 2019). Following the synchrotron burst, experimental measurements (near-edge photoabsorption spectroscopy, resonant Auger electron spectroscopy, X-ray photoelectron spectroscopy, and mass spectrometry) were used along with computational modeling to study how the chemical environment affects the excitation, ionization and fragmentation of the molecule. It is possible that their approach may be used to study how Auger processes are affected by the local environment in even

more complex biomolecules such as DNA. Synchrotron approaches were also undertaken by Boudjemia et al. (Boudjemia et al. 2019). They induced photoionization of the iodine 1s and 2s shells of iodomethane (CH_3I) and trifluoroiodomethane (CF_3I). Their results were analyzed using theoretical relativistic molecular and atomic computational models. They observed charge redistribution within deep electronic levels in the molecule and the redistribution was depended on the number of electron vacancies. Analysis of the Auger spectra provided information on the distribution of charge in the molecules. Quantum electrodynamics corrections were required to predict core shell binding energies in these molecules that include heavy atoms. More importantly, their work on charge distribution inside molecules demonstrated that electronegative iodine atoms can draw charge from the rest of the molecule at an extremely rapid rate. Furthermore, this ultrafast process plays a role in doubly charged atoms (as in Auger decay) even for the deep levels encountered in LMX Auger transitions. These finding strongly support the Charlton/AAPM method of continuous replenishment of electrons when simulating Auger cascade processes to calculate radiation spectra for Auger electron emitters in tissue environments (Charlton and Booz 1981; Howell 1992).

Fukuzawa et al. used a near-infrared X-ray free-electron laser (XFEL) with femtosecond time resolution to induce electronic decay in diiodomethane molecules (Fukuzawa et al. 2019). The lifetimes of the transient states populated during the XFEL-induced Auger cascades were determined. Singly charged iodine ions were found to originate from longer-lived states (~100 fs), whereas multiply charged ions arose from short-lived (~20 fs) transient states. Furthermore, during the molecular fragmentation process, the long- and short-lived states relax predominantly by interatomic Coulombic decay between two iodine atoms and molecular Auger decay, respectively.

Interestingly, measurements of single, double and triple Auger decay (Figure 3) were made after creation of a core vacancy in C, N, and O atoms, and CO and CO_2 molecules (Roos et al. 2016; Roos et al. 2018; Hult Roos et al. 2019). Triple Auger decay occurred with a probability of about 100-fold less than single Auger decay. The fraction of double Auger decay depended linearly on the number of valence electrons in the atom in which the initial core vacancy was created and in adjacent neighbors. This led to very high probabilities (20–30%) of double Auger decay in molecules such as CCl_4 and SF_6. Therefore, these modes of decay likely play an important role in high Z atoms in molecules. Müller et al. also conducted measurements of single, double and triple Auger decay following the creation of K-shell vacancies in carbon (Muller A et al. 2015). The relative cross sections for these processes in C^{1+} were approximately 97:3:0.01). This finding may have implications for Monte Carlo simulations of Auger electron spectra that arise when Auger electron emitting radionuclides decay within biomolecular structures.

Pronschinske et al. created two-dimensional [125]I Au-supported monolayers which facilitate the study of how radiation interacts with atoms in 2-dimensional molecular layers (Pronschinske et al. 2016). The elemental composition of these monolayers changes continuously because of the nuclear transmutation of ^{125}I to [125]Te. They found that the Auger electrons emitted have kinetic energies commensurate with those of neutral tellurium. They discovered that newly formed Te reacted to become TeO_2 and then was dimerized.

Furthermore, the Te_2O_4 units remained intact during major lateral rearrangement of the monolayer. This suggest remarkable stability of the dimer. Notably, their results provide insight into the composition and mobility of surface species in a radioactive monolayer with an atomic-scale spatial resolution. This may have implications for the radiobiology of Auger electron emitters.

Atomic physics is moving rapidly with the capability to observe attosecond-scale atomic rearrangements using laser technology. Pulse-laser technology facilitates probing of subfemtosecond transient population of short-lived valence electronic states in excited atoms or molecules. It provides the capacity to observe ultrafast multi-electron dynamics during Auger and ICD transitions that occur on a timescale ranging from attoseconds to femtoseconds.

These attosecond pulse techniques have been used to show that when valence electron is ejected, the electron hole can migrate from one end of the molecule to another extremely fast. The fate of electrons after a core ionization is another matter. Kuleff et al. have demonstrated that when a hole is created in the core shells, the hole does not migrate but there is prolific charge migration in the valence shell (Kuleff et al. 2016). The pace of migration of these valence electrons is faster when a core hole is created than when a valence electron is ejected. Furthermore, the pace of migration is much faster than the natural decay of the core hole by the Auger process. This suggests that Monte Carlo simulations of Auger electron cascades should replenish valence electrons when calculating Auger electron spectra for radiopharmaceutical dosimetry. This approach was developed by Charlton and adopted by Howell in the AAPM report (Charlton and Booz 1981; Howell 1992).

Ferreira et al. studied ionization of water with energy transfers close to the 2a1 inner valence orbital (Ferreira et al. 2017). These energy transfers were associated with fast electronic rearrangement driven by electron relaxation and electron–electron correlations. Exciting states are created in outer shells consisting of quasi-degenerate single vacancies and one-electron-two-vacancy excited states. Auger decay and double ionization arise from single vacancy states. Satellite excited states are associated with single ionization. Specifically, the fragmentation of water into $H^0 + O^+ + H^0$ by electron impact results in H^0 ejections leaving the O^+ almost at rest. In summary, Auger processes are involved in the evolution of radical species produced following the radiolysis of water and relevant to modeling molecular damage caused by indirect effects.

Kai et al. have created a Monte Carlo code that simulates the dynamic behavior of low-energy secondary electrons produced by Auger electrons in water (Kai et al. 2016a). The code accounts for the Coulombic force between parent cations and the secondary electrons ejected therefrom. The decelerating electrons are often attracted to within several nm of their parent cations within hundreds of femtoseconds. If this process takes place inside a cell, lesions may form around a cation created within a DNA molecule via dissociative electron transfer, ionization, and electronic excitation. These, in turn, may cause mutations or cell killing (Kai et al. 2016a, 2016b; Kai et al. 2018).

Allum et al. have studied the dynamics of Coulomb explosion of gaseous CH_3I and CH_2CII following atomic rearrangements created by ultrashort laser pulses (Allum et al. 2018). Specifically, the ultrafast (i.e. femtosecond) dissociations of the C–I bond in these molecules were studied using time-resolved Coulomb explosion imaging that can determine the kinetic energy releases of the fragment ions. These studies are helpful in elucidating the probabilities and associated time scales of competing processes that lead to different ion fragments.

When high-Z nanoparticles are irradiated with external beams of radiation, interatomic Coulomb decay electrons and Auger electrons (0–1000 eV) are emitted. Jeon et al. measured the production of reactive oxygen species around irradiated iron oxide nanoparticles that lie within three-dimensional gels (Jeon et al. 2016). The confocal laser scanning technique measures the range and distribution of ●OH and superoxide anions O_2^- produced by low-energy electrons. This interesting approach was used in the context of X-irradiated nanoparticles but could also be used by mixing an Auger electron emitting radionuclide into the gel and observing the radical species created around the decay site.

Ultimately, the collection of new techniques described above are important for understanding the radiobiological effects of Auger processes. These include improvements in the accuracy of transition rates and energies for N- and O-shell transitions, the dependence of Auger transition rates and energies on molecular effects, and how to handle vacancies when modeling the Auger cascade process. Of significant need are experimental data specifically for the radionuclides of interest in both atomic and molecular form. This would permit validation of computer models that are used to calculate Auger electron spectra.

Low Energy Electron Irradiator

Kumar et al. have developed a device to irradiate biomolecular films with low energy electrons (Kumar et al. 2016). Samples can be irradiated under ultrahigh vacuum sat preset electron energy and absorbed doses. The irradiator holds up to 7 samples which are not hit by stray electron irradiation because a bias of −20 V is applied when the sample is not being irradiated. The irradiator was used to induced SSB ΦX174 RF1 dsDNA with electron energies ranging from 0.5 to 500 eV. This is an excellent resource for low energy electron radiobiology.

Cellular and Multicellular Dosimetry

Cellular absorbed dose is an important metric that has been used to establish the positional dependence of the high-LET nature of Auger electron cascades. MIRDcell was released in 2014 to facilitate cellular and multicellular dosimetry calculations that are required for internal radionuclides (Figure 4) (Vaziri et al. 2014). Since its release, numerous studies have been undertaken to compare Monte Carlo track structure computational approaches with the analytical approach used in MIRDcell. For example, Cai et al. compared the absorbed doses calculated with MCNP and MIRDcell for the theragnostic radionuclide [64]Cu (Cai Z et al. 2017). It emits positrons (40% yield), Auger electrons, internal conversion (IC) electrons, and photons. They concluded that the absorbed doses calculated with MCNP and

MIRDcell were in reasonable agreement for the most part. However, there were significant differences for cross-doses that were calculated for some radionuclides when they were distributed in the cytoplasm or on the cell surface. MCNP was also used by Taborda et al. to calculate S-values for ^{99m}Tc in single mouse thyroid follicles (Taborda et al. 2016). They included photon contributions and found that photons and ^{99m}Tc Auger electrons contributed equally to the absorbed dose. The equal contribution by Auger-electrons suggest that they play an important role in murine thyroid stunning effect caused by ^{99}Tc radiopharmaceuticals.

Šefl et al. used Geant4-DNA to study how geometry of a cell affects S value calculations for monoenergetic electron (1 to 100 keV) emitters localized in different subcellular compartments (Sefl et al. 2015). The same distributions were considered for the Auger-electron emitting radionuclides ^{99m}Tc, ^{111}In, and ^{125}I. The cell geometries studied included a sphere and an ellipsoid, each with the same cellular and nuclear volume. Their S values differed from those in the MIRD Cellular S Values monograph (Goddu et al. 1997) by as much as 50%. However, most differences were less than 10%. Similar results were obtained by Moradi and Bidabadi (Seifi Moradi and Shirani Bidabadi 2018). The S values for the ellipsoidal cell geometry were typically within 20% of the value for spherical geometry; the largest difference was about 32% (Sefl et al. 2015). These results are similar to calculations for ellipses in the MIRD monograph and those of Nettleton (Nettleton and Lawson 1996; Goddu et al. 1997). Differences between spherical and irregular geometries were greatest (100–300%) when activity was localized on the cell surface. They pointed out that the AAPM spectra for ^{125}I were published in two different places which yielded differences of up to 19% in cellular S values. Howell and Emfietzoglou traced this problem in 2013 (personal communication). The correct original print copy was published in Medical Physics 19(6) 1371–1383 (1992) and reproduced in Table 1 (I-125 correct) of Šefl et al. (Howell 1992; Sefl et al. 2015). AAPM had character-recognition scanned this document and used it along with other documents to create a web version of the complete AAPM Report 37 comprised of three documents. The character scanned version did not reproduce the tables of Auger electron yields and energies accurately. This incorrect version was reproduced in Table 1 (I-125 incorrect) of Šefl et al. (Sefl et al. 2015). In 2013, at the request of Howell, AAPM deleted the erroneous version and created a web link to the original version of the radiation spectra for Auger electron emitters (Howell 1992). In agreement with the conclusions in the MIRD Cellular S Value monograph, Šefl et al. stated cellular S values for Auger electron emitters in elliptically shaped cells is typically reasonably approximated by calculations using spherical geometry (within 20–30%). However, caution should be exercised when using the spherical approximation for radionuclides distributed on the surface of cells.

Siragusa et al. developed the COmputation Of Local Electron Release (COOLER) software that can perform dosimetry at the cellular/subcellular scale for Auger electron emitters distributed in various cell compartments (Siragusa et al. 2017). This MATLAB program uses mathematical fits to electron energy deposition values that were calculated using the PARTRAC Monte Carlo track structure code. Cellular S value predictions were calculated for uniform activity in the cell, cell nucleus, or on the surface of the cell. These were compared to S values calculated directly with PARTRAC, and with MIRDcell V2.0.15

(Vaziri et al. 2014). The largest discrepancies between COOLER and MIRDcell V2.0.15 S values were for electrons having energies of 25–30 keV. In these cases, differences of 50–100% were obtained for radioactivity distributed on the surface of the cell. The software, which can also be used for dosimetry modeling of suspension and adherent cell culture geometries, can be downloaded at http:www.nutech.dtu.dk/.

Significant differences in cross-doses have also been calculated for geometries involving eccentric nuclei (Falzone et al. 2019). The effects of cell eccentricity on S values was determined for cell with different combinations of radii for the cell and cell nucleus. The S values calculated with PENELOPE were typically within 10% of MIRD for S(nucleus←nucleus). Larger differences were obtained for S(nucleus←cytoplasm) and S(nucleus←cell surface). As expected, eccentricity had the largest effect on the S value for small nuclei relative to the size of the cell, and for cell surface distributions. Similar calculations were undertaken by Salim & Taherparvar using Geant4-DNA with similar results (Salim and Taherparvar 2019).

Lee et al. used the Particle and Heavy Ion Transport code System (PHITS) to calculate S values for cell and tumor metastasis containing ^{212}Pb, ^{225}Ac, ^{213}Bi, ^{90}Y, ^{177}Lu and ^{111}In (Lee D et al. 2018). As observed by them and in the MIRD Cellular S Value tables, moving the radioactivity from cell surface to cell cytoplasm to cell nucleus has a major effect on increasing the value of the S value. The S values calculated with PHITS matched the MIRDcell S values (cellular S values) and the tumor S values calculated by Hindié et al. (Vaziri et al. 2014; Hindie et al. 2016). Given that most radiopharmaceuticals do not localize in a single cell compartment, a notable capability of their cellular dosimetry approach is to enable the subcellular distribution to be split between compartments (i.e. nucleus, cytoplasm, cell surface).

Carter et al. have developed the PARaDIM program that uses tetrahedral mesh-type phantoms for absorbed dose calculations (Carter et al. 2019). The software can implement most alpha, beta, gamma, positron, and Auger/conversion electron emitters of relevance to diagnostic and therapeutic nuclear medicine. It calculates mean absorbed dose using PHITS Monte Carlo track structure approaches to designated regions and three-dimensional absorbed dose distributions. They demonstrated the versatility of the program by calculating absorbed doses for human, small-animal, and cells. PARaDIM and OLINDA 2.0 agreed to within 10%−20% for most organs. PARaDIM and MIRDcell were within 5% for most cellular S values. This program can be downloaded at www.paradim-dose.org.

Differences in cellular S values are most often attributed to Monte Carlo versus point kernel computational approaches. However, differences in radiation spectra are often overlooked. Falzone et al. recently studied how radiation input spectra affects calculation of cellular S values for Auger electron emitters (Falzone et al. 2017). The yield of Auger and CK electrons released per decay in the MIRD-RADTABS files were consistently higher than those calculated using *BrIccEmis*. Accordingly, dose point kernels calculated with *BrIccEmis* spectra were quite different from those calculated with the MIRD-RADTABS data, particularly within a few hundred nm of the decay site. Cellular S values were not significantly affected by the source of the spectrum as the differences in dose point kernels

over nm dimensions were quickly diminished upon reaching cellular dimensions. Therefore, these two sources of radiation spectra for Auger electron emitters are equally appropriate for cell level dosimetry whereas caution must be exercised when selecting radiation spectra for molecular dosimetry. In contrast, Fourie et al. calculated S values for ^{123}I with several different Monte Carlo dosimetry programs and indicated that differences in S values can be largely attributed to the source of the radiation spectrum (Fourie et al. 2015). Care must also be taken for cell-level dosimetry of low-energy beta emitters where the full radiation spectra are needed (Goddu et al. 1997).

While cellular dosimetry offers a simple means to relate biological response to absorbed dose, the high RBE of DNA-incorporated Auger electron emitters is clear indication that the relevant absorbed doses are at the nanometer scale (Sastry and Rao 1984). Accordingly, Di Maria et al. created S values for subnuclear target volumes corresponding to chromosomes and other small structures within the cell (Di Maria et al. 2018). These S values can be used when activity distributions are measured at subcellular spatial scales. As the target volume decreases, the S values increase rapidly compared to the MIRD cellular S values (Goddu et al. 1994; Goddu et al. 1997).

Reijonen et al. created a multicellular dosimetry program that uses voxelized geometry (Reijonen et al. 2017). The model was built upon segmented confocal microscope images of a spheroid. Nonuniform activity distributions were simulated by adjusting the fraction of cell nuclei that contain either ^{111}In, ^{125}I, or ^{177}Lu. The absorbed dose was calculated with vxlPen which is based on PENELOPE. They determined that the cross-irradiation afforded by ^{177}Lu beta particles confers a relatively uniform dose distribution when 60% of the cells are labeled. However, the short-range nature of the Auger electrons emitted by ^{111}In and ^{125}I made the fraction of cells labeled a major factor in the absorbed dose distribution. These and other dependencies can be examined quickly on the MIRDcell platform mentioned above.

Raghavan et al. developed a theoretical multicellular dosimetry model that folds in the dynamics of diffusion and its effects on the absorbed dose distribution of radiopharmaceuticals (Raghavan et al. 2017). The model is intended to accommodate a new form of radiopharmaceutical administration, namely convection-enhanced delivery (CED). In this approach, a device is used to exert pressure to infuse a radiopharmaceutical through a tissue boundary (e.g. infusion into tissue margins of the cavity formed upon resecting a glioma). The model integrates fluid flow and radiation dose models to study how various parameters affect the dose distributions of radiopharmaceuticals comprised of Auger electron-emitting radionuclides. They demonstrated that Auger electron emitters would provide substantial normal tissue sparing making them superior to longer range alpha particle emitters and beta particle emitters for convection-enhanced delivery.

Cellular absorbed dose calculations generally assume uniform distribution of radioactivity in cell compartments. The exact location of the decays is generally not well-known. Experiments and modeling have been conducted determine the spatial distribution of decays in the cell using photoresist autoradiography (PAR) (Royle et al. 2015; Royle et al. 2016). The model correlates the location and fluence of the source with the depth and radius (in the x-y plane) of the PAR pattern. A good fit to experimental data was obtained.

Therefore, the combination of PAR measurements and modeling can be used to pinpoint the subcellular location of the decay sites created by Auger electron emitting radionuclides in the cell. These details could be integrated into more detailed dosimetric calculations at the subcellular level.

DNA damage by Auger processes

The DNA damage caused by Auger processes induced by external beams of ionizing radiation and using radionuclides that emit Auger electrons has been a key topic particularly because of the highly localized energy deposition (HILED) imparted by these low-energy electrons (Sastry KSR 1992). Over the past four years, DNA-damage caused by Auger processes has been assessed *in vitro* using plasmid and cell culture models, as well as *in silico* studies using Geant4-DNA. These studies are summarized below.

Othman et al. compared the cytotoxicity of ^{67}Ga-oxine and ^{111}In-oxine with the intent of demonstrating the viability of ^{67}Ga as a therapeutic Auger electron emitter (Othman et al. 2017). These agents were tested in DU145 prostate cancer cells, and MDA-MB-231 and HCC1954 breast cancer cell lines from human patients. They concluded that these Auger electron emitters produce equivalent damage to plasmid DNA in solution and similar cell kill when equal amounts activity are taken up by the cell. This is interesting considering that ^{67}Ga and ^{111}In have average yields of 4.7 and 14.7 Auger electrons per decay, respectively (Howell 1992), although the somewhat longer physical half-life of ^{67}Ga results in more intracellular decays for the same initial activity and ^{67}Ga delivers a higher absorbed dose to the nucleus per decay in the nucleus than ^{111}In (0.0036 versus 0.0027 Gy Bq^{-1} s^{-1} based on MIRDcell calculations with cell and nucleus radii of 6 and 4 μm, respectively (Vaziri et al. 2014)). Othman et al. have suggested that ^{67}Ga should be evaluated further for therapeutic applications (Othman et al. 2017).

Reissig et al. made ^{99m}Tc-labeled pyrene derivatives that are DNA intercalators (Reissig et al. 2016). The derivatives had different distances between the pyrene moiety and ^{99m}Tc. These were used to label pUC 19 plasmid DNA and the resulting DNA fragments were quantified. Experiments were then conducted to assess DNA damage in the presence and absence of dimethyl sulfoxide (DMSO), a radical scavenger. The ^{99m}Tc Auger electrons created DNA single strand breaks (SSB) and double strand breaks (DSB) and the molecular damage was only partially prevented by DMSO. The direct effect (i.e. DMSO present) was mitigated by increasing the distance between ^{99m}Tc and the pyrene moiety. In related studies, Pereira et al. synthesized several ^{99m}Tc-tricarbonyl complexes and ^{125}I-heteroaromatic compounds that contained a DNA intercalating unit (acridine orange (AO)) and evaluated their potential for radiopharmaceutical therapy (Pereira et al. 2017). As expected, both classes of compounds cause DSB in DNA and the extent of the damage depended on the distance between the AO moiety and the Auger electron emitter. The ^{125}I-C5 and ^{99m}Tc-C3 configurations provided similar distances between the radionuclide and DNA and yielded about the same yield of DSB in both plasmids and cellular DNA. The DSB/decay was extremely low (0.02–0.04 DSB/decay) compared to that obtained by others when ^{125}I is incorporated into the DNA with ^{125}I-iododeoxyuridine (~ 1 DSB/decay). Their interpretation of the results is that ^{125}I and ^{99m}Tc decays produce about the same

amount DNA damage when they are positioned at about the same distance from DNA. This is surprising considering historical data that suggests that proportionally more decays are required to achieve the same biological effect from a radionuclide that emits few Auger electrons compared to one that emits many Auger electrons (see Discussion).

Lobachevsky et al. investigated the Auger/positron-emitter [124]I which has a shorter half-life (4.18 d) than the longer-lived Auger electron emitter [125]I (60 d) (Lobachevsky et al. 2016). They compared the capacity of the two radionuclides to impart biological damage as quantified by DNA DSB per decay. Attaching the radionuclides to plasmid DNA with para-[[124]I]/[^{125}I]-iodoHoechst yielded an average of 0.58 and 0.85 DSB per decay for [124]I and ^{125}I, respectively. These studies, supported by in vivo biodistribution data, support the use of [124]I-labeled DNA ligands for theragnostic radiopharmaceutical therapy.

Piroozfar et al. conducted Geant4-DNA modeling studies on how distance from DNA affects direct induction of DSBs by [111]In Auger cascades (Piroozfar et al. 2018). They studied the effectiveness of Auger electron energy on the efficiency of causing DSB. Geant4-DNA predicted that 183 eV electrons would be most effective, but the high yield of 350 eV electrons could be attributed to most of the DSBs. Their results indicate that ^{111}In produces about ~1.3 DSBs per decay when placed within 4 nm of the central axis of DNA. This value was commensurate with that of earlier experiments (Sahu et al. 1995).

Tomita et al. investigated induction of DSB and cell killing following ionization from the K-shell of phosphorus (Tomita et al. 2016). Several human cell lines were exposed to monochromatic synchrotron X-rays with energies above and below the K-edge of phosphorus (2153 or 2147 eV). Greater biological effects, quantified by 53BP1/c-H2AX co-localized foci, G2 arrest, and cell killing, were observed when irradiating above the K-edge (2153 eV). Thus, they attributed the enhanced biological effects of 2153 keV synchrotron X-rays to the cascade of Auger electrons that follow K-shell photoabsorption in phosphorus.

Cellular DNA damage and gene expression

Schmitz et al. analyzed chromatid aberrations after human peripheral blood lymphocytes were labeled with [125]IUdR for 18 h (Schmitz et al. 2015, 2016). Only 40% of the cells were labelled, to a high degree, another 20% moderately labeled, and 40% unlabeled. The lowest absorbed dose delivered was 0.2 Gy and this caused a thirteen-fold increase in aberrations compared to the unlabeled controls. Their data indicates that DNA-incorporated ^{125}I produces ~ 0.2 chromatid aberrations per decay.

Dahmen et al. used ^{125}I-labeled triplex-forming oligonucleotides (TFO) to bind to DNA at site-specific locations (Dahmen et al. 2017). The Auger electron emitter ^{125}I can introduce complex radiation-induced DNA lesions at specific sites that are susceptible to chromosomal translocations (Panyutin and Neumann 1994). In addition to aberrations, Dahmen et al. studied translocation frequency, and changes in gene and protein expression after transfecting ^{125}I-labeled TFO-BCL2 into SCL-II cells (Dahmen et al. 2017). The TFO-BCL2 binds to the BCL2 gene near a major breakage region. The measured translocation frequency of BCL2 t(14;18) yielded a two-fold increase when compared to controls

indicating that ^{125}I decays facilitated the translocation which contributed to enhancement of BCL2 gene expression.

Unverricht-Yeboah conducted gene expression analyses after exposing Jurkat cells to intracellularly incorporated ^{123}IUdR, as well as external beams of α-particles and γ-rays (Unverricht-Yeboah et al. 2018). At equieffective exposure to these radiation sources, 155, 316 and 982 genes were regulated, respectively. Candidate genes were narrowed down to discriminate between damage caused by the different sources. Four genes (PPP1R14C, TNFAIP8L1, DNAJC1 and PRTFDC1) were needed to reliably discriminate between γ- and ^{123}IUdR exposure, one gene (KLF10) was needed to discriminate between γ- and α-radiation, and one gene (TNFA/P8L1) was needed to discriminate between α- and ^{123}IUdR exposure. These results are supported by those of Sokolov et al. (Sokolov et al. 2006). This suggests that changes in the expression of these genes may serve as radiation-quality specific biomarkers.

Extranuclear Radiosensitive Targets and Bystander Effects

Maucksch et al. studied three ^{99m}Tc-labeled diagnostic radiopharmaceuticals with different subcellular distributions, namely ^{99m}Tc-pertechnetate, ^{99m}Tc-hexamethyl-propylene-aminoxime (^{99m}Tc-HMPAO) and ^{99m}Tc-hexakis-2-methoxyisobutylisonitrile (^{99m}Tc-MIBI) (Maucksch et al. 2016). ^{99m}Tc-HMPAO showed the highest uptake in the cell nucleus of rat thyroid FRTL-5 cells, whereas lower nuclear uptake was observed for ^{99m}Tc-pertechnetate and ^{99m}Tc-MIBI. Cell survival was assessed using the colony-forming assay which revealed D_{37} values of 3.6, 4.1, and 13.6 Gy, respectively. However, quantitation of DNA damage with γH2AX did not demonstrate similar behavior. Given, that ^{99m}Tc-HMPAO was also taken up highly by the cell membrane/organelles, they have suggested that extra-nuclear radiosensitive targets may play a role in cell killing by ^{99m}Tc-HMPAO.

Ladjohounlou et al. studied radiation-induced bystander effects caused by the alpha particle emitters ^{212}Pb/^{212}Bi and ^{213}Bi, and the Auger electron emitter ^{125}I (Ladjohounlou et al. 2019). Studies were conducted both in vitro and in vivo with an intent for using them in radioimmunotherapy (RIT). They found that 7–36% and about 28% of the cells were killed by bystander effects caused by the alpha emitters and Auger electron emitter, respectively. Bystander effects were partly driven by cell membrane–mediated effects and their radiotoxicity could be modulated with drugs that affect cholesterol level such as statins.

Paillas et al. studied radiation-induced bystander effects caused by ^{125}I-labeled monoclonal antibodies (^{125}I-mAbs) that localize on the surface of cells (Paillas et al. 2016). The toxicity in p53$^{+/+}$ HCT116 colon cancer cells was attributed largely to bystander effects. The underlying mechanisms involved activation of acid-sphingomyelinase which led to ceramide enriched domains in the lipid rafts on the cell membrane, that in turn modulated AKT, ERK1/2, p38 kinase, and JNK signaling pathways ending in cell death (Figure 5). It also involved PLC-c, PYK-2, paxillin, and the flux of Ca^{2+}. Interestingly, the bystander response induced by ^{125}I-mAb was similar to responses elicited by DNA-incorporated ^{125}I-iododeoxyuridine. These in vitro results were supported by further studies in vivo. Their results indicate that targeting the cancer cell surface with ^{125}I-mAbs can elicit bystander

effects that compensate for the inferior efficacy of direct irradiation when the Auger emitting radiopharmaceutical is localized outside of the cell nucleus.

As pointed out recently by Leung et al., no single definition fits the nature of the bystander conditions that are present in radiopharmaceutical therapy (Leung et al. 2020). While these statements were in the context of ^{223}Ra therapy, the same reasoning applies to Auger electron emitters. Most Auger electron emitters typically emit a mixture of radiations including gamma rays, x rays, conversion electrons, and Auger electrons. These radiations irradiate neighboring cells at distances that depend on the spectrum of radiations emitted. The absorbed dose received by the neighboring cells and the cellular organelles that are hit also depend on the location of the decay sites in the radiolabeled cells. An Auger electron emitter localized on the cell membrane will always irradiate at least the membrane and cytoplasm of the nearest neighbors. The MIRDcell software tool, including Multicellular Geometry < 1-D Cell Pair tab and the Output tab, is useful to interactively study these dependencies (Vaziri et al. 2014). The "classical" definition of bystander effects indicates that they are responses of unirradiated cells to signals that are elicited upon irradiating nearby cells (Blyth and Sykes 2011). Cohort effects are the responses of a population of irradiated cells that are not attributed to direct radiation hits (Blyth and Sykes 2011). Both these effects can be transmitted via released factors and/or gap junctional intercellular communication. When radiation-induced effects arise in locations very far from the region irradiated, they have been coined abscopal effects. These 3 classes of effects are often referred to as "nontargeted" in the context of external-beam radiobiology in the sense that radiation hits are not directly responsible for some of the observed effect. However, the use of the term "targeted" in radiopharmaceutical therapy refers to physical localization of the radiopharmaceutical to a specific population of cells or treatment region. The "targeted" cells will irradiate themselves and the surrounding cells. Therefore, those surrounding cells may not be "targeted" by the radiopharmaceutical but they are "targeted" by the radiation emanating from the "targeted" cells. This conundrum makes it confusing to use "nontargeted effects" in the context of radiopharmaceutical therapy. In the Leung et al. article, we suggest that the totality of these effects be called bystander effects in the sense that an irradiated cell (tumor and normal) can impart effects to other cells that may or may not have been irradiated (Leung et al. 2020). This terminology is consistent with clinical implementation of radiopharmaceutical therapy, in which cells are irradiated while the radiopharmaceutical circulates throughout the body and concentrates in the tumor, making it unlikely that there are cells that are not irradiated at all. Key to this, and recognized by others, is the understanding that a bystander is a cell that may have been either irradiated or unirradiated and a bystander effect is one that is imparted from irradiated cells (Blyth and Sykes 2011; Brady et al. 2013). The capacity to kill bystanders will be particularly helpful for radiopharmaceuticals labeled with Auger electron emitters.

Therapeutic aspects of Auger processes

Falzone et al. studied how nonuniform distributions of Auger electron emitters in multicellular spheroids affects tumor control probability (Falzone et al. 2019). Spheroids were created in vitro with MDA-MB-468, SQ20B, and 231-H2N cells (Figure 6). These were exposed to ^{111}In-EGF or ^{111}In-trastuzumab and intratumoral distribution

was determined by microautoradiography. Clonogenic cell survival was used as the experimental model to assess cytotoxicity. A theoretical dose-response model was created using a close-packed algorithm that randomly packs cells with different radii of cells and nuclei into a 3-dimensional spheroid model. Calculated surviving fractions were generated based on absorbed doses calculated with PENELOPE. The theoretical and experimental surviving fractions were compared along with tumor control probabilities. Calculated surviving fractions agreed with experimental surviving fractions when an RBE was used for the self-dose to the nucleus. Only ^{111}In-EGF afforded a tumor control probability greater than 0.5 for MDA-MB-468 spheroids. The subcellular and macroscopic distribution of Auger electron emitters has a major impact on tumor control probability. Therefore, multicellular level dosimetry is essential for predicting the capacity of Auger emitting radiopharmaceuticals to sterilize micrometastases. It also puts a premium on selecting radiopharmaceuticals that can penetrate into the spheroid. Major improvements in penetration capacity have been made by Zhu et al. using pH sensitive liposomes (Figure 7) (Zhu C et al. 2017).

The use of nanoparticles containing high-Z elements has matured into a topic of major interest in external beam radiotherapy. Numerous investigators have demonstrated increased radiotoxicity of photon beams when high-Z nanoparticles are introduced into cells prior to irradiation with photon beams. Auger electrons, generated in the aftermath of ejecting inner shell electrons from the high-Z element, have been attributed to the enhanced radiotoxicity observed. Antosh et al. used pH Low-Insertion Peptide (pHLIP) to bind gold nanoparticles to the cell membrane of cancer cells (Antosh et al. 2015). The pHLIP labeled the cells profusely with gold particles which increased killing of the cells upon irradiation with 250 kVp X-rays with Sn-Thoraeus filtering.

Cai et al. labeled gold nanoparticles (AuNP) with ^{111}In-trastuzumab (trastuzumab-AuNP-^{111}In) using polyethylene glycol chains as linkers (Cai Z et al. 2016). They assessed their effects on cultured HER2-positive breast cancer cells and when the agent was administered to xenografts via an intratumoral injection. The radiopharmaceutical complex was internalized into breast cancer cells in greater amount than AuNP-[111]In. The trastuzumab-AuNP-^{111}In complex had a much greater effect on surviving fraction and tumor growth than AuNP-[111]In. Their results suggest that Auger electron emitting antibody gold nanoparticle complexes may be useful local treatment of HER2-positive breast cancer.

Modalities for treating prostate cancer include ^{125}I seeds which irradiate the tumor with low energy γ and x-rays. Chan et al. used these photons to ionize selenium nanoparticles (SeNPs) that were targeted to cancer cells (Chan et al. 2017). The ^{125}I photons and the Auger cascades induced by them in Se atoms work synergistically to inhibit cell growth and cell survival. Detailed mechanistic studies suggest that the combined treatments activate overproduction of intracellular reactive oxygen species that regulate p53- mediated apoptotic signaling pathways and mitogen activated protein kinase (MAPK) phosphorylation and to prevent repair. This form of photon activation therapy, pioneered by Fairchild (Fairchild and Bond 1984), offers an interesting strategy for therapy in clinical applications.

Delorme et al. studied the dose-enhancement afforded by isolated gadolinium atoms or gadolinium nanoparticles (GdNPs) upon irradiation with monochromatic x-rays (Delorme et al. 2017). This in silico study was complemented with clonogenic cell survival assays after treating the cells with either Magnevist (gadolinium contrast agent (GdCA)) or GdNPs. The treated cells were "irradiated" with 30–80 keV monochromatic X-rays or high energy ^{60}Co gamma rays. The Monte Carlo simulations projected copious production of low energy electrons around the GdNPs when they were irradiated with a beam energy above the K-edge of gadolinium. The emission of low-energy electrons increases the local absorbed doses dramatically which can be used to induce cell death. Different intracellular distributions of gadolinium were investigated. The dose enhancement for nuclear localization was lower than those for localization in the cytoplasm or cell membrane. Radiosensitization was provided by GdNPs irradiated at all energies. Although simulated dose enhancement factors were lower than experimental values, both followed similar trends when beam energy was changed.

Gill et al. labeled nanoparticles with ^{111}In and drugs for cancer cell targeting (Gill et al. 2018). They conjugated DTPA-hEGF (human epidermal growth factor) or a ruthenium-based DNA replication inhibitor and radiosensitizer Ru(phen)2(tpphz)2+ Ru1 to the surface of poly (lactic-co-glycolic acid) (PLGA) nanoparticles. ^{111}In-labeled PLGA were taken up by EGFR-overexpressing esophageal cancer cells and radiotoxicity was observed. The PGLA labeled with both Ru1 and ^{111}In caused more cell killing than single-agent formulations. Their work demonstrated that combinations of Auger electron emitters and chemical agents carried to tumor cells with nanoparticles can be an effective approach for therapy.

Grudzinski et al. synthesized ^{125}I-labeled 18-(p-iodophenyl) octadecylphosphocholine (CLR1404), an alkyl-phosphocholine analog, and tested its antitumor efficacy in nude mice bearing either MDA-MB-231-luc triple negative breast cancer lung metastases or orthotopic xenografts (Grudzinski et al. 2018). Pharmacokinetic measurements and dosimetry indicated that ^{125}I-CLR1404 delivers high tumor doses and very low doses to bone marrow, thereby giving it a good safety profile. ^{125}I-CLR1404 reduced tumor volume by 60% relative to vehicle control and it extended the life of the animals. It also inhibited the progression of micrometastases making it a promising candidate for radiopharmaceutical therapy of micrometastases of triple negative breast cancers.

Kiess et al. irradiate cancer cells with Auger electrons emitted by ^{125}I-labeled prostate-specific membrane antigen (PSMA; ^{125}I-DCIBzL) (Kiess et al. 2015). DNA damage and clonogenic survival caused by this agent were assessed with PSMA-positive (PSMA$^+$) PC3 PIP and PSMA-negative (PSMA$^-$) PC3 flu human prostate cancer cells. Antitumor efficacy was tested against PSMA$^+$ or PSMA$^-$ xenografts in mice. Increased DNA damage and decreased clonogenic survival was observed in PSMA$^+$ cells compared with PSMA$^-$ cells. Correspondingly, the PSMA$^+$ tumors exhibited greater growth delay than PSMA$^-$tumors Therefore, ^{125}I-DCIBzL is a promising radiopharmaceutical for treating micrometastases of prostate cancers (Figure 8).

Kortylewicz et al. studied a radioiodine-labeled androgen receptor targeting agent 5-radioiodo-30-O-(17b-succinyl-5a-androstan-3-one)-20-deoxyuridin-50-yl phosphate (RISAD-P) for theragnostic treatment of AR-expressing prostate cancer (Kortylewicz et al. 2015). The RISAD-P molecule was labeled with ^{123}I, [124]I, or ^{125}I and their therapeutic efficacies and normal tissue toxicity were evaluated in mice. RISAD-P excellent tumor targeting and did not produce normal tissue toxicity at doses projected for theragnostic use in the clinic. Tumor uptake was rapid with almost 10% of the injected activity in the tumor within one hour post-administration of ^{125}I-RISAD-P. Tumor clearance was biphasic and flattens 24 to 48 h post-administration. Radiation absorbed doses were estimated for a 1 g tumor using standard MIRD conventions. The absorbed doses were therapeutic with values of 170, 250, 1240 Gy MBq^{-1} for [125]I-, [123]I-, and [124]I-labeled RISAD-P, respectively. The high tumor doses and low doses to normal tissues make radioiodinated RISAD-P very suitable for imaging AR expression and for radiopharmaceutical therapy of metastatic to regionally advanced prostate cancer. Furthermore, Auger-electron-emitting radiopharmaceuticals based on hormonal receptors such as the androgen receptor could be attractive, since these receptors translocate to the cell nucleus upon ligand binding, and may localize the Auger electron emitter in close proximity to the DNA.

Miran et al. evaluated pharmacological glutathione (GSH) depletion as a means to radiosensitize breast cancer stem cells to radiopharmaceutical therapy with ^{125}I–labeled 5-iodo-49-thio-29-deoxyuridine ([125]ITdU) (Miran et al. 2017; Miran et al. 2018). Cancer stem cells were defined as CD242⁻ and CD44⁺. Buthionine sulfoximine (BSO) was used to inhibit GSH synthesis in mice with CD242⁻ and CD44⁺ xenografts. The mice received weekly injections of [125]ITdU. Complete tumor regression was observed when the animals were preconditioned with BSO prior to treatment with [125]ITdU. Their results suggest that GSH modulation in DNA-incorporating Auger electron emitting radiopharmaceuticals, such as [125]ITdU, may afford the possibility of sterilizing drug-resistant cancer stem cells.

Slastnikova et al. has synthesized modular nanotransporters (MNTs) to direct Auger electron emitters to folate-receptors (FR) on the cell surface and transport them into the cell nucleus (Slastnikova, Rosenkranz, Khramtsov, et al. 2017). They used this approach to deliver the Auger electron emitter ^{111}In into the nuclei of target FR-expressing HeLa human cancer xenografts in mice (Figure 9). These tumor studies showed that the agent afforded prolonged retention of ^{111}In and significant growth inhibition. These studies, and those of Rosencranz et al. (Rosenkranz et al. 2018), suggests that FR-targeted MNT may be suited for radiopharmaceutical therapy with Auger electron emitters.

Thisgaard et al. used a convection-enhanced delivery approach to treat small glioblastoma spheroid cultures and orthotopic glioblastoma xenografts in rats with [125]IUdR (Thisgaard et al. 2016). The [125]IUdR was administered in the absence and presence of the chemotherapeutic agents methotrexate or temozolomide. In spheroids, the [125]IUdR decreased cell migration and viability. Co-treatment with methotrexate and/or temozolomide impacted these endpoints further. Convection enhanced delivery of [125]IUdR, when administered along with temozolomide, reduced glioblastoma xenograft burden in nude rats and all treated animals survived for 180 days. This level of success could not be achieved

with either agent alone. These findings suggest that convection enhanced delivery of a cocktail of chemotherapeutics and [125]IUdR is a promising option for glioblastoma therapy.

Photon activation therapy was studied by Corde et al. (Corde et al. 2004) who discovered that there is an unexpected optimal photon energy for activating IUdR to enhance the radiotoxicity of x-rays. They found that 50 keV photons are most effective for increasing radiotoxicity. This energy far above the 33.169 keV K-edge of iodine. Monoenergetic x-rays with energies slightly above the iodine K edge were less effective. Bayart et al. have followed up on this finding and have shown that the enhanced radiotoxicity of photon activation of IUdR with photons with a mean energy of 50 keV is due to increased DNA-damage whose repair is impaired (Bayart et al. 2017). This and prior studies reviewed by Yokoya & Ito (Yokoya and Ito 2017), indicate that beam characteristics will play a key role in clinical implementation of photon activation therapy.

Chemo-Auger combination therapy of cancer is a therapeutic approach that involves labeling a chemotherapy agent with an Auger electron emitter (Hou et al. 1985; Howell et al. 1986; Azure et al. 1992). Bleomycin, daunorubicin, and doxorubicin have been studied for chemo-Auger combination therapy (Ghirmai et al. 2005; Haefliger et al. 2005; Hafliger et al. 2005; Jaaskela-Saari et al. 2005; Ickenstein et al. 2006; Schipper et al. 2007). Following the work of these and others, Imstepf et al. have coupled ^{99m}Tc to the chemotherapeutic agent doxorubicin (Imstepf et al. 2015). The ^{99m}Tc-doxorubicin inhibited cell survival in a dose-dependent manner. A biodistribution study in healthy mice found that the radiolabeled drug uptake in organs was comparable to that of the parent drug (Imstepf et al. 2015). However, the low Auger electron yield of ^{99m}Tc and the short physical half-life (6 h) are such that very high injected activities would be required to attain a high degree of tumor cell kill. The prevalent photon yield then delivers high cross-doses to organs in the body. This was the case in the studies of Schipper et al. which achieved good tumor control but considerable normal tissue toxicity (Schipper et al. 2007).

Radioimmunotherapy (RIT) with Auger electron emitters has been evolving over decades. Bergstrom et al. investigated Auger RIT of acute myeloid leukemia (AML) with ^{111}In-DTPA-NLS-CSL360 (Bergstrom et al. 2016). Two experimental models were used: 1) non-obese diabetic severe combined immunodeficiency (NOD/SCID) mice, and 2) NODRag1[null]IL2rγ[null] (NRG) mice engrafted with CD123^{+} human AML-5 cells. Paradoxically, ^{111}In-DTPA-NLS-CSL360 and ^{111}In-DTPA-NLS-hIgG increased the fraction of hCD45^{+} bone marrow cells of NOD/SCID mice despite anticipated radiation-induced suppression of leukemic cells in the bone marrow. The authors suggested that irradiation of the marrow with ^{111}In may have primed the BM niche in the same manner that occurs when γ-radiation is used to permit the AML engraftment. There appears to be a competition between this apparent leukemia engraftment enhancement effect and the cytotoxic effect caused by irradiating the leukemia cells with the Auger electrons. The authors also found that the efficacy of the therapy depended on the leukemic burden. These results may have implications when evaluating radioimmunotherapies for application in patients with AML (Bergstrom et al. 2016).

Gao et al. prepared a radiolabeled chimeric IgG$_1$ monoclonal antibody (CSL360) that binds to CD123$^+$/CD131$^-$ leukemic stem cells (LSC) (Gao et al. 2016). As in the study above, the ^{111}In-DTPA-NLS-CSL360 radioimmunoconjugate has an NLS which transports the radionuclide to the nucleus of human AML-5 myeloid leukemia cells. Survival of AML-5 cells treated with the agent was reduced substantially whereas cell survival was unaffected by unlabeled CSL360, DTPA-NLS-CSL360 and free ^{111}In acetate. These results suggest that ^{111}In-DTPA-NLS-CSL360 may be useful in treating AML.

Song et al. recognized that the specific activity of radiolabeled antibodies and peptides often limits their therapeutic efficacy (Song et al. 2016). Accordingly, they radiolabeled ^{111}In to EGF-gold nanoparticles (^{111}In-EGF-Au NP) at high specific activity. Clonogenic cell survival was used to assess cytotoxicity of the conjugate. Due to increased EGFR expression on MDA-MB-468 compared to MCF-7 cells, the former was significantly more sensitive to ^{111}In-EGF-Au NP. This approach to increase the payload of Auger electron emitters such as ^{111}In to cancer cells may be a good avenue in the continued development molecularly targeted radiotherapy.

Ngo et al. increased specific activity of the targeting agent by modifying trastuzumab with a metal-chelating polymer (MCP) that contains multiple copies of DTPA to chelate ^{111}In (Ngo Ndjock Mbong et al. 2015). The MCPs were created with 24 or 29 pendant DTPA groups and an NLS and attached to the Fc-domain of trastuzumab (tTrastuzumab-HyMCP-^{111}In). For comparison, trastuzumab was also modified to include two DTPA chelates and then labeled with ^{111}In (trastuzumab-NH-Bn-DTPA-^{111}In). As expected, trastuzumab-HyMCP-^{111}In was found in the nucleus of SK-BR-3 cells. However, intranuclear localization was not increased with NLS bearing MCPs. Increasing the specific activity with MCPs increased the cytotoxicity of ^{111}In trastuzumab against HER2-overexpressed and gene-amplified BC cells. It also was able to kill cells with intermediate HER2 expression and cells overexpressing HER2 but resistant to trastuzumab. Given the heterogeneous expression of HER2 in tumor cells in any given patient, this approach has the capacity overcome some of the therapeutic limitations imposed by this phenomenon (Neti and Howell 2006; Pasternack et al. 2014).

Razumienko et al. also created radiopharmaceuticals to overcome trastuzumab resistance in HER2$^+$ breast cancer. They created ^{111}In-labeled bispecific radioimmunoconjugates (bsRICs) by linking Fab fragments of trastuzumab to EGF with polyethylene glycol (PEG24). This permitted targeting of tumors that are HER2$^+$ EGFR$^+$ with a single molecule labeled with a radionuclide. ^{177}Lu- and ^{111}In-labeled trastuzumab Fab or EGF killed tumor cells that expressed HER2 or EGFR, respectively, whereas radiolabeled bsRICs were able to kill cells that displayed HER2 or EGFR or both. The bsRICs were more cytotoxic than monospecific agents. Animals studies demonstrated a 2-fold increase in tumor uptake of ^{177}Lu-DOTA-Fab-PEG24-EGF compared to ^{177}Lu-DOTA-trastuzumab Fab or ^{177}Lu-DOTA-EGF. The beta particle emitting ^{177}Lu-DOTA-Fab-PEG24-EGF was more effective at inhibiting tumor growth than ^{111}In-DTPA-Fab-PEG24-EGF because it delivered a tumor absorbed dose of 55.0 Gy vs. the 5.9 Gy delivered by the latter. These results confirm that macroscopic tumors are often better treated with beta emitters than Auger

electron emitters (Howell et al. 1989), and that dual-receptor–targeted radioimmunotherapy of cancer with bsRICs may increase tumor uptake of the radiopharmaceutical.

Optimal Radionuclide

Among the many considerations for therapy with Auger electron emitters is selecting the best radionuclide for the task. This topic has been discussed extensively in the literature. In that vein, is worthwhile to review the calculations of Uusijärvi et al. who evaluated the capacity of many Auger electron emitters to irradiate tumor tissue while sparing normal tissues (Uusijärvi et al. 2006). Their analysis suggested that the best Auger electron emitters for therapy on the basis of dosimetry are ^{58m}Co, ^{189m}Os, ^{103m}Rh, ^{193m}Pt, and ^{195m}Pt, with ratios of absorbed dose rate to small tumor and normal tissue of 89, 64, 36, 26, and 25, respectively when localized in the cell nucleus. The platinum radionuclides emit an average of more than *30* Auger electrons per decay and they are extremely radiotoxic when delivered into the cell nucleus (Howell et al. 1986; Azure et al. 1992; Howell et al. 1994). New methods to produce high specific activity radioplatinum were discussed at the present Oxford meeting. Therefore, further progress in the therapeutic use of these platinum radionuclides is anticipated.

Duchemin et al. have promoted the use of terbium radionuclides such as ^{155}Tb, an Auger electron emitter, for therapeutic applications (Duchemin et al. 2016). This radionuclide decays by electron capture with a physical half-life of 5.3 d and, by virtue of its high atomic number, produces a sizeable shower of Auger electrons. They produced ^{155}Tb with 34 MeV deuterons and measured the excitation function of the ^{nat}Gd(d,x)^{155}Tb reaction and of the produced terbium and gadolinium contaminants. The acquired data constitutes an addition to the database for the ^{nat}Gd(d,x) reaction and information that can be used to optimize the irradiation conditions required to produce high-purity ^{155}Tb.

Hindie et al. compared the capacity of ^{90}Y, ^{177}Lu, ^{111}In, and ^{161}Tb to irradiate micrometastases (Hindie et al. 2016). ^{90}Y and ^{177}Lu are high- and medium-energy beta emitters. ^{161}Tb emits medium-energy β$^-$ particles with energies similar to ^{177}Lu but its yield of conversion and Auger electrons is higher. Of course, ^{111}In emits both conversion electrons and Auger electrons. A program called CELLDOSE was used to calculate absorbed doses when these radionuclides are uniformly distributed spheres of water with diameters ranging from 10–10000 μm. They concluded that the combination medium-energy β– particles and Auger electrons emitted by ^{161}Tb may enhance its therapeutic applicability (Champion et al. 2016).

Another Auger electron emitter, ^{135}La, has been proposed for Auger-based targeted internal radiotherapy (Fonslet et al. 2017). ^{135}La was produced by irradiating metallic ^{nat}Ba with 16.5 MeV protons to achieve a radionuclidic purity of 98%. Chemical separation yielded high specific activity ^{135}La 70 GBq μmol^{-1} with excellent yield. The ^{135}La decays almost entirely to the ground state of stable ^{135}Ba, with a physical half-life 18.9 h. Monte Carlo simulation of the ensuing Auger cascade predicted an average yield of 10.6 Auger electrons per decay. Using MIRDcell v2.1 (Vaziri et al. 2014), the calculated cellular S values (cell radius = 7 μm, nucleus radius = 5 μm, and nucleus is source and target) for ^{135}La are about 20% lower than those for the well-studied ^{111}In. Therefore, its utility as a therapeutic

radionuclide will depend largely on any advantages related to its ease of radiolabeling and chemical stability of the resulting radiopharmaceutical in vivo.

Selection of the best Auger electron emitting radionuclide for therapy is an optimization process. Many variables are relevant such Auger electron yield per decay (generally affects number of decays needed to inactivate a cell), physical half-life, photon yield to facilitate imaging without imparting undue cross irradiation, availability of isotopes that emit only beta particles for purposes of comparison, ease of production in carrier free form, chemical properties as it relates to preparation of radiochemicals and their stability in vivo, etc. It is a long list with plenty of room for optimizing beyond what has been achieved thus far. Regardless of the choice of the Auger electron emitter, due to the low cross-irradiation and relatively low mean energy emitted per decay (of particulate radiations) associated with most prolific Auger electron emitters, therapeutic radiopharmaceuticals labeled with Auger electron emitters are likely to require higher administered activities than typical therapeutic beta particle emitters to reach comparable equieffective doses (Behr et al. 2000; Bentzen et al. 2012).

Other Related Articles

This author apologizes for omitting a large number of other contemporaneous research articles on aspects directly and indirectly related to Auger processes are not mentioned above due to space limitations (Cai H et al. 2015; Chudzicki et al. 2015; Fasshauer et al. 2015; Frolova et al. 2015; Ghosh et al. 2015; Gierz et al. 2015; Giovanni et al. 2015; Giussani 2015; Gorobtsov et al. 2015; Herve du Penhoat et al. 2015; Iskandar et al. 2015; Leyton et al. 2015; Li HK et al. 2015; Li Z et al. 2015; Liekhus-Schmaltz et al. 2015; Liu P et al. 2015; Martinez-Rovira and Prezado 2015; McMillan et al. 2015; Panosa et al. 2015; Peters et al. 2015; Protti et al. 2015; Rakowski et al. 2015; Slastnikova et al. 2015; Taupin et al. 2015; Vaxenburg et al. 2015; Walther et al. 2015; Wang C et al. 2015; Wang H et al. 2015; Wragg et al. 2015; Xie et al. 2015; Zhang et al. 2015; Bourque et al. 2016; Cho et al. 2016; Dahmen et al. 2016; Dong et al. 2016; Feifel et al. 2016; Gessner and Guhr 2016; Goldsztejn, Marchenko, Ceolin, et al. 2016; Goldsztejn, Marchenko, Puttner, et al. 2016; Haller et al. 2016; He et al. 2016; Iablonskyi et al. 2016; Iwayama et al. 2016; Kaminaga et al. 2016; McMahon et al. 2016; McNamara et al. 2016; Mikell et al. 2016; Moser et al. 2016; Mukherjee et al. 2016; Murray et al. 2016; Nagaya, Iablonskyi, et al. 2016; Nagaya, Motomura, et al. 2016; Peng et al. 2016; Reissig et al. 2016; Retif et al. 2016; Roteta et al. 2016; Runge et al. 2016; Sann et al. 2016; Spencer et al. 2016; Sung et al. 2016; Tang et al. 2016; Terrissol 2016; Violet et al. 2016; Watanabe et al. 2016; Yasui et al. 2016; Yokoya 2016; Chirayath et al. 2017; Hans et al. 2017; Heuskin et al. 2017; Iablonskyi et al. 2017; Jablonski and Powell 2017; Kaneyasu et al. 2017; Lechtman and Pignol 2017; Liu XJ et al. 2017; Miteva et al. 2017; Nicolas et al. 2017; Paro et al. 2017; Sisourat, Engin, et al. 2017; Sisourat, Kazandjian, et al. 2017; Slastnikova, Rosenkranz, Morozova, et al. 2017; Spencer et al. 2017; Sreedharan et al. 2017; Takanashi et al. 2017; Travnikova et al. 2017; Valdovinos et al. 2017; Vultos et al. 2017; Won et al. 2017; Yokoya and Ito 2017; You et al. 2017; Fukunaga et al. 2018; Grokhovsky 2018; Guerreiro et al. 2018; Maucksch et al. 2018; Nicolas et al. 2018; Oehme et al. 2018; Qaim and Spahn 2018; Righi et al. 2018; Santos et al. 2018; Shinohara et al. 2018; Taha et al. 2018; Kelbg et al. 2019; Kojima et

al. 2019; Kotzerke et al. 2019; Li et al. 2019; Muller C et al. 2019; Sakata et al. 2019; Villagomez-Bernabe and Currell 2019; Xu et al. 2019; Zhu Y et al. 2019). The interested reader should study these articles as well.

The Future of Auger Processes in Biology and Medicine

During the 2015–2019 period covered by this review, advances have been made in our understanding of the physics of Auger cascades, the radiobiological responses to Auger electron emitting radiopharmaceuticals, and their application in cancer therapy. DNA-damage by Auger processes has always been an important area of research in this field. No other source of radiation can target DNA and other radiosensitive sites with the same precision as Auger electrons. In prior years, experiments have been conducted to probe how the radiotoxicity of the prolific Auger electron emitter ^{125}I depends on distance from the DNA molecule (Balagurumoorthy et al. 2012). By deftly manipulating the distance between ^{125}I decay and the plasmid, a sharp transition between direct high-LET type effects and low-LET type indirect effects were observed. The new studies of Reissig et al. and Pereira et al., summarized in sections above, have extended this approach to an Auger electron emitter with a much lower electron yield per decay, namely ^{99m}Tc (Reissig et al. 2016; Pereira et al. 2017). The latter study directly compared ^{99m}Tc and ^{125}I and found comparable effects when located at the same distance from the plasmid. However, the DSB/decay were very low and therefore the authors conclusion that ^{99m}Tc-labelled acridine orange derivatives are more promising for therapy than the ^{125}I-labeled congeners is perhaps premature. It may be difficult to deliver the requisite number of decays of ^{99m}Tc that are required to inactivate cells while keeping normal tissue doses from photons and conversion electrons at an acceptable level (Schipper et al. 2007). This is addressed in the section entitled Optimal Radionuclide.

Relevant to this discussion is the work of Kassis and co-workers who have shown that the RBE (at 37% survival) of the Auger cascades produced by ^{77}BrUdR, ^{123}IUdR, and ^{125}IUdR are all ~ 7 when compared with gamma rays delivered acutely with a ^{137}Cs irradiator (Kassis et al. 1982; Kassis et al. 1987; Makrigiorgos et al. 1989). These Auger cascades took place at the same molecular location on the DNA. Notably, ^{77}Br, ^{123}I, and ^{125}I emit an average 7, 15, and 24 Auger electrons per decay, respectively (Howell 1992). The number of decays required to kill 63% of the cells were 120, 277, and 366, respectively (Kassis et al. 1982; Kassis et al. 1987; Makrigiorgos et al. 1989). Therefore, while more decays are required to achieve the same mean absorbed dose to the cell nucleus when a low number of Auger electrons are emitted, their relative biological effectiveness is about the same when they are emitted by radionuclides similarly incorporated into the DNA. The bottom line here is that maximizing the Auger electron yield per decay minimizes the number of decays required to kill the cell and therefore our focus should be predominantly on prolific Auger electron emitters.

Indeed, therapeutic applications of Auger electrons that address the issue of delivering sufficient decays to inactivate targeted cells were a major focus of this meeting. One way to achieve high therapeutic effect with a minimum number of radioactive decays is to localize the Auger electron emitter in the cell nucleus, preferably intercalated or incorporated into

the DNA. Major advances have been made in the development of radiopharmaceuticals that facilitate both accurate targeting of cancer cells and taking the Auger electron emitter into the cell nucleus using nuclear localizing sequences (Ngo Ndjock Mbong et al. 2015; Bergstrom et al. 2016; Gao et al. 2016; Slastnikova, Rosenkranz, Khramtsov, et al. 2017). These technologies leverage the high-LET type radiotoxicity that Auger electron emitters can impart thereby minimizing the number of decays required to achieve the desired therapeutic effect. However, while the effectiveness of these approaches were demonstrated by these authors in vitro with cultured cells, and in vivo with intratumoral injections, further advances are needed to develop such radiopharmaceuticals that can be intravenously administered and enter the nucleus of the target cells without having undergone degradation in the circulatory system or upon entering the target cells.

As mentioned above, there are viable alternatives to relying solely on direct irradiation of nuclear DNA with Auger electrons. Among them are targeting other cellular organelles, and also radiation-induced bystander effects. For example, Auger electron emitters targeted to the cell membrane deposit most of their energy at the cell surface. However, the Auger cascades that take place on the membrane activate intracellular signaling that leads to secondary generation of nuclear damage (Figure 5) (Paillas et al. 2013; Piron et al. 2014). The cell death that follows cannot be explained in terms of absorbed dose to the nucleus, thereby highlighting the cell membrane as an important target in the context of Auger electron emitters. Radiation-induced bystander effects are also an important strategy to harness for radiopharmaceutical therapy with Auger electron emitters. Auger-induced bystander effects are elicited not only by DNA-incorporated Auger electron emitters (Howell and Bishayee 2002; Xue et al. 2002; Pouget et al. 2008; Paillas et al. 2016; Ladjohounlou et al. 2019), but also when the radionuclide is localized on the cell membrane (Santoro et al. 2009; Boudousq et al. 2010; Paillas et al. 2013; Piron et al. 2014). These Auger-induced bystander effects are an important tool to help overcome problems associated with nonuniform activity distributions.

Inactivating tumor cell populations with the minimum number of decays is related to another important challenge that must be overcome to successfully use Auger electron emitters to weaponize radiopharmaceuticals against cancer, namely lognormal uptake of radiopharmaceuticals by tumor cells. Log normal distributions of radiopharmaceutical uptake in cell populations is the norm and this can profoundly impact the ability of a radiopharmaceutical to sterilize a population of tumor cells (Neti and Howell 2006). Such distributions are attributed to the natural lognormal distribution of target receptors in targeted radiopharmaceutical therapy, but it also manifests for chemotherapy agents and other pharmaceuticals that can be labeled with Auger electron emitters. This problem is most significant to this class of radionuclides because their radiotoxicity can be attributed largely to the high self-dose to the labeled cells, although radiation-induced bystander effects can overcome this to some extent as mentioned above. Creating radiopharmaceutical strategies that target cell populations with Auger electron emitters more uniformly may ultimately be the most effective therapeutic agents because they are more likely to minimize normal tissue toxicity by reducing the amount of administered activity needed to achieve maximum therapeutic effect. To visualize the impact of such nonuniform distributions of Auger electron emitters (or alpha and beta emitters) on the surviving fraction of cells in

2-dimensional and 3-dimensional populations of cells, the reader can download and run the software tool MIRDcell (Vaziri et al. 2014). This easy to use tool has an array of features that are ideal for calculating absorbed doses to each cell of a multicellular population and predicting the fraction of surviving cells.

Another avenue for overcoming the negative impact of nonuniform activity distributions on therapeutic outcome is the novel liposome technology of Zhu et al. (Zhu C et al. 2017). Their pH sensitive liposomes penetrate multicellular spheroids and deliver encapsulated radiopharmaceuticals to cells far inside (Figure 7). Cocktails of radiopharmaceuticals, and perhaps chemotherapy agents, can also provide the coverage needed to label and sterilize a cell population (Akudugu et al. 2011; Akudugu and Howell 2012b, 2012a; Pasternack et al. 2014; Thisgaard et al. 2016). Key to the radiopharmaceutical cocktail approach is the specific activity of the individual radiopharmaceuticals that comprise the cocktail (Pasternack et al. 2014). Advancement of strategies that increase the uniformity of labeling tumor cells is necessary in the design of Auger radiopharmaceutical therapy, photon activation therapy, and high-Z nanoparticle external beam therapies.

There has been a substantial amount of new work on calculating Auger electron spectra that arise from electron capture, internal conversion, and photon activation in molecular environments. However, new computational models are needed to account for single, double and triple Auger decay and ICD (Roos et al. 2016; Roos et al. 2018; Hult Roos et al. 2019). The fractions of double Auger decay are linearly dependent on the number of valence electrons in the atom with the initial core vacancy and in its neighbors. This leads to very high probabilities (20–30%) of double Auger decay in molecules such as CCl_4 and SF_6. Even higher percentages are expected for high Z atoms that are used for Auger radiopharmaceuticals. Furthermore, the new evidence for attosecond transfer of electrons from neighboring atoms suggests that continuous electron filling of valence shells is needed when performing Monte Carlo simulations of Auger cascades (Kuleff et al. 2016). Lastly, experimental validation of the very low energy electrons comprised in Auger electron spectra is needed.

While the focus of Auger therapies have been largely focused on cancer, the capacity of Auger electron emitters to irradiate specific molecular sites can be used by other scientific fields. Kurt Hofer suggested that Auger electron emitters may be used to study aging (Hofer 1992). Recently, senolytic agents are being used in an attempt to reduce the adverse effects of aging and prevent recurrence of cancer in patients that have undergone therapy (Kirkland et al. 2017; Saleh et al. 2020). Auger electron emitters may be the perfect payload for such agents because of their short-range and high-LET radiotoxicity. They may also offer some level of safety over alpha particle emitters which are potent carcinogens. In another arena, Panyutin et al. considered Auger electron emitters for gene therapy (Panyutin and Neumann 1994; Panyutin et al. 2000). In these instances where deft implementation of site-specific irradiation is needed, radionuclides that decay by electron capture directly to the daughter ground state may be most suitable. These radionuclides emit only Auger electrons and low yields of characteristic x-rays. There are few such radionuclides with suitable physical half-lives, perhaps [71]Ge may be ideal with a half-life of 11.4 d. Therefore, there remains a rich future to study DNA repair of site-specific radiation damage.

Auger electron cascades deposit an unparalleled density of energy. Local absorbed doses can exceed 1 MGy which can lead to very high RBE values that can exceed those of alpha particles (Howell et al. 1990; Rao et al. 1990; Howell et al. 1991; Sastry KS 1992). Extensive studies carried out over decades prompted international organizations that assess dosimetry and radiation risks to provide more guidance on handling Auger electron emitters. For example, in Annex B of the 2007 ICRP recommendations and ICRU Report 86, the issues surrounding the radiotoxicity of Auger electron emitters are addressed in more depth than previous reports by these international bodies (ICRP 2007; ICRU 2011). These reports recognize the low-LET type behavior when Auger electron emitters are directed to cytoplasmic targets but their extreme high-LET type radiotoxicity when incorporated into DNA in the cell nucleus. They recommended taking account of the potential for high-LET type radiotoxicity individually for each radiopharmaceutical. Given our increased understanding of the radiobiological effects of Auger electron emitters, there is room to develop more prescriptive approaches that require details regarding the chemical structure of the radiopharmaceutical and its subcellular distribution.

In conclusion Auger electrons can deliver highly localized doses of radiation within 10 nm of the decay site. This make them precision tools for discovery across the physical, chemical, biological and medical sciences. Only a relative few curious scientists have ventured into Auger space and they have learned a great deal. However, much remains to be discovered so there is plenty to do for new scientists interested in the field.

Acknowledgments

References

Adelstein SJ. 1992. Biophysical apsects of Auger processes: A review of the literature 1987–1991. In: Howell RW, Narra VR, Sastry KSR et al., editors. Biophysical Aspects of Auger Processes. Woodbury, NY: American Institute of Physics (http://www.aapm.org/pubs/books/PROC_8.pdf); p. 1–13.

Aghevlian S, Boyle AJ, Reilly RM. 2017. Radioimmunotherapy of cancer with high linear energy transfer (LET) radiation delivered by radionuclides emitting alpha-particles or Auger electrons. Adv Drug Deliv Rev. 109:102–118. [PubMed: 26705852]

Akudugu JM, Azzam EI, Howell RW. 2012. Induction of lethal bystander effects in human breast cancer cell cultures by DNA-Incorporated Iodine-125 depends on phenotype. Int J Radiat Biol. 88(12):1028–1038. Eng. [PubMed: 22489958]

Akudugu JM, Howell RW. 2012a. Flow cytometry-assisted Monte Carlo simulation predicts clonogenic survival of cell populations with lognormal distributions of radiopharmaceuticals and anticancer drugs [Research Support, N.I.H., Extramural]. Int J Radiat Biol. 88(3):286–293. eng. [PubMed: 22054423]

Akudugu JM, Howell RW. 2012b. A method to predict response of cell populations to cocktails of chemotherapeutics and radiopharmaceuticals: Validation with daunomycin, doxorubicin, and the alpha particle emitter ^{210}Po. Nucl Med Biol. 39(7):954–961. eng. [PubMed: 22503536]

Akudugu JM, Neti PVSV, Howell RW. 2011. Changes in lognormal shape parameter guide design of patient-specific radiochemotherapy cocktails. J Nucl Med. 52(4):642–649. [PubMed: 21421713]

Allum F, Burt M, Amini K, Boll R, Kockert H, Olshin PK, Bari S, Bomme C, Brausse F, Cunha de Miranda B et al. 2018. Coulomb explosion imaging of CH3I and CH2ClI photodissociation dynamics. The Journal of chemical physics. 149(20):204313. [PubMed: 30501230]

Alotiby M, Greguric I, Kibedi T, Lee BQ, Roberts M, Stuchbery AE, Tee P, Tornyi T, Vos M. 2018. Measurement of the intensity ratio of Auger and conversion electrons for the electron capture decay of (125)I. Phys Med Biol. 63(6):06NT04.

Antosh MP, Wijesinghe DD, Shrestha S, Lanou R, Huang YH, Hasselbacher T, Fox D, Neretti N, Sun S, Katenka N et al. 2015. Enhancement of radiation effect on cancer cells by gold-pHLIP. Proc Natl Acad Sci U S A. 112(17):5372–5376. [PubMed: 25870296]

Auger P 1923. Sur les rayons β secondaires produits dans un gaz par des rayons X. Comptes rendus de l'Académie des Sciences. 177:169–171.

Azure MT, Sastry KSR, Archer RD, Howell RW, Rao DV. 1992. Microscale synthesis of carboplatin labeled with the Auger emitter Pt-193m: Radiotoxicity versus chemotoxicity of the antitumor drug in mammalian cells. In: Howell RW, Narra VR, Sastry KSR et al., editors. Biophysical Aspects of Auger Processes. Woodbury, NY: American Institute of Physics (https://www.aapm.org/pubs/books/PROC_8.pdf); p. 336–351.

Balagurumoorthy P, Xu X, Wang K, Adelstein SJ, Kassis AI. 2012. Effect of distance between decaying (125)I and DNA on Auger-electron induced double-strand break yield. Int J Radiat Biol. 88(12):998–1008. [PubMed: 22732063]

Barth S, Joshi S, Marburger S, Ulrich V, Lindblad A, Ohrwall G, Bjorneholm O, Hergenhahn U. 2005. Observation of resonant interatomic coulombic decay in Ne clusters. The Journal of chemical physics. 122(24):241102. eng. [PubMed: 16035737]

Bavelaar BM, Lee BQ, Gill MR, Falzone N, Vallis KA. 2018. Subcellular Targeting of Theranostic Radionuclides. Frontiers in pharmacology. 9:996. [PubMed: 30233374]

Baverstock KF, Charton DE, editors. 1988. DNA Damage by Auger Emitters. London: Taylor & Francis.

Bayart E, Pouzoulet F, Calmels L, Dadoun J, Allot F, Plagnard J, Ravanat JL, Bridier A, Denoziere M, Bourhis J et al. 2017. Enhancement of IUdR Radiosensitization by Low-Energy Photons Results from Increased and Persistent DNA Damage. PLoS One. 12(1):e0168395. [PubMed: 28045991]

Behr TM, Behe M, Lohr M, Sgouros G, Angerstein C, Wehrmann E, Nebendahl K, Becker W. 2000. Therapeutic advantages of Auger electron- over beta-emitting radiometals or radioiodine when conjugated to internalizing antibodies. European journal of nuclear medicine. 27(7):753–765. [PubMed: 10952487]

Bennett K, Kowalewski M, Mukamel S. 2015. Probing electronic and vibrational dynamics in molecules by time-resolved photoelectron, Auger-electron, and X-ray photon scattering spectroscopy. Faraday discussions. 177:405–428. [PubMed: 25730500]

Bentzen SM, Dorr W, Gahbauer R, Howell RW, Joiner MC, Jones B, Jones DT, van der Kogel AJ, Wambersie A, Whitmore G. 2012. Bioeffect modeling and equieffective dose concepts in radiation oncology - Terminology, quantities and units. Radiother Oncol. 105(2):266–268. [PubMed: 23157980]

Bergstrom D, Leyton JV, Zereshkian A, Chan C, Cai Z, Reilly RM. 2016. Paradoxical effects of Auger electron-emitting ^{111}In-DTPA-NLS-CSL360 radioimmunoconjugates on hCD45^{+} cells in the bone marrow and spleen of leukemia-engrafted NOD/SCID or NRG mice. Nuclear medicine and biology. 43(10):635–641. [PubMed: 27497632]

Bishayee A, Rao DV, Bouchet LG, Bolch WE, Howell RW. 2000. Radioprotection by DMSO against cell death caused by intracellularly localized I-125, I-131, and Po-210. Radiat Res. 153:416–427. [PubMed: 10761002]

Bizau JM, Cubaynes D, Guilbaud S, Penent F, Lablanquie P, Andric L, Palaudoux J, Al Shorman MM, Blancard C. 2016. Photoelectron Spectroscopy of Ions: Study of the Auger Decay of the 4d-->nf (n=4,5) Resonances in Xe5+ Ion. Physical review letters. 116(10):103001. [PubMed: 27015477]

Blyth BJ, Sykes PJ. 2011. Radiation-induced bystander effects: what are they, and how relevant are they to human radiation exposures? [Research Support, U.S. Gov't, Non-P.H.S. Review]. Radiat Res. 176(2):139–157. eng. [PubMed: 21631286]

Bolognesi P, Carravetta V, Sementa L, Barcaro G, Monti S, Manjari Mishra P, Cartoni A, Castrovilli MC, Chiarinelli J, Tosic S et al. 2019. Core Shell Investigation of 2-nitroimidazole. Frontiers in chemistry. 7:151. [PubMed: 31001511]

Boros E, Holland JP. 2018. Chemical aspects of metal ion chelation in the synthesis and application antibody-based radiotracers. Journal of labelled compounds & radiopharmaceuticals. 61(9):652–671. [PubMed: 29230857]

Boros E, Packard AB. 2019. Radioactive Transition Metals for Imaging and Therapy. Chemical reviews. 119(2):870–901. [PubMed: 30299088]

Boudjemia N, Jankala K, Gejo T, Nagaya K, Tamasaku K, Huttula M, Piancastelli MN, Simon M, Oura M. 2019. Deep core photoionization of iodine in CH3I and CF3I molecules: how deep down does the chemical shift reach? Physical chemistry chemical physics : PCCP. 21(10):5448–5454. [PubMed: 30793147]

Boudousq V, Ricaud S, Garambois V, Bascoul-Mollevi C, Boutaleb S, Busson M, Quenet F, Colombo PE, Bardies M, Kotzki PO et al. 2010. Brief intraperitoneal radioimmunotherapy of small peritoneal carcinomatosis using high activities of noninternalizing 125I-labeled monoclonal antibodies. J Nucl Med. 51(11):1748–1755. [PubMed: 20956481]

Bourque JL, Biesinger MC, Baines KM. 2016. Chemical state determination of molecular gallium compounds using XPS. Dalton Trans. 45(18):7678–7696. [PubMed: 27052931]

Bradley EW, Chan PC, Adelstein SJ. 1975. The radiotoxicity of iodine-125 in mammalian cells. I. Effects on the survival curve of radioiodine incorporated into DNA. Radiat Res. 64:555–563. [PubMed: 1197658]

Brady D, O'Sullivan JM, Prise KM. 2013. What is the Role of the Bystander Response in Radionuclide Therapies? Frontiers in oncology. 3:215. [PubMed: 23967404]

Cai H, Singh AN, Sun X, Peng F. 2015. Synthesis and characterization of Her2-NLP peptide conjugates targeting circulating breast cancer cells: cellular uptake and localization by fluorescent microscopic imaging. Journal of fluorescence. 25(1):113–117. [PubMed: 25620472]

Cai Z, Chattopadhyay N, Yang K, Kwon YL, Yook S, Pignol JP, Reilly RM. 2016. ^{111}In-labeled trastuzumab-modified gold nanoparticles are cytotoxic in vitro to HER2-positive breast cancer cells and arrest tumor growth in vivo in athymic mice after intratumoral injection. Nuclear medicine and biology. 43(12):818–826. [PubMed: 27788375]

Cai Z, Kwon YL, Reilly RM. 2017. Monte Carlo N-Particle (MCNP) Modeling of the Cellular Dosimetry of 64Cu: Comparison with MIRDcell S Values and Implications for Studies of Its Cytotoxic Effects. J Nucl Med. 58(2):339–345. [PubMed: 27660146]

Carter LM, Crawford TM, Sato T, Furuta T, Choi C, Kim CH, Brown JL, Bolch WE, Zanzonico PB, Lewis JS. 2019. PARaDIM: A PHITS-Based Monte Carlo Tool for Internal Dosimetry with Tetrahedral Mesh Computational Phantoms. J Nucl Med. 60(12):1802–1811. [PubMed: 31201251]

Cederbaum LS, Zobeley J, Tarantelli F. 1997. Giant intermolecular decay and fragmentation of clusters. Physical review letters. 79(24):4778.

Champion C, Quinto MA, Morgat C, Zanotti-Fregonara P, Hindie E. 2016. Comparison between Three Promising ss-emitting Radionuclides, [67]Cu, [47]Sc and [161]Tb, with Emphasis on Doses Delivered to Minimal Residual Disease. Theranostics. 6(10):1611–1618. [PubMed: 27446495]

Chan L, He L, Zhou B, Guan S, Bo M, Yang Y, Liu Y, Liu X, Zhang Y, Xie Q et al. 2017. Cancer-Targeted Selenium Nanoparticles Sensitize Cancer Cells to Continuous gamma Radiation to Achieve Synergetic Chemo-Radiotherapy. Chemistry, an Asian journal. 12(23):3053–3060. [PubMed: 28892302]

Charlton DE, Booz J. 1981. A Monte Carlo treatment of the decay of I-125. Radiat Res. 87:10–23. [PubMed: 7255664]

Chirayath VA, Callewaert V, Fairchild AJ, Chrysler MD, Gladen RW, McDonald AD, Imam SK, Shastry K, Koymen AR, Saniz R et al. 2017. Auger electron emission initiated by the creation of valence-band holes in graphene by positron annihilation. Nature communications. 8:16116.

Cho J, Gonzalez-Lepera C, Manohar N, Kerr M, Krishnan S, Cho SH. 2016. Quantitative investigation of physical factors contributing to gold nanoparticle-mediated proton dose enhancement. Phys Med Biol. 61(6):2562–2581. [PubMed: 26952844]

Chudzicki M, Werner WS, Shard AG, Wang YC, Castner DG, Powell CJ. 2015. Evaluating the Internal Structure of Core-Shell Nanoparticles Using X-ray Photoelectron Intensities and Simulated Spectra. The journal of physical chemistry C, Nanomaterials and interfaces. 119(31):17687–17696. [PubMed: 26339331]

Corde S, Joubert A, Adam JF, Charvet AM, Le Bas JF, Esteve F, Elleaume H, Balosso J. 2004. Synchrotron radiation-based experimental determination of the optimal energy for cell radiotoxicity enhancement following photoelectric effect on stable iodinated compounds. British journal of cancer. 91(3):544–551. eng. [PubMed: 15266326]

Dahmen V, Pomplun E, Kriehuber R. 2016. Iodine-125-labeled DNA-Triplex-forming oligonucleotides reveal increased cyto- and genotoxic effectiveness compared to Phosphorus-32. Int J Radiat Biol. 92(11):679–685. [PubMed: 27022855]

Dahmen V, Schmitz S, Kriehuber R. 2017. Induction of the chromosomal translocation t(14;18) by targeting the BCL-2 locus with specific binding I-125-labeled triplex-forming oligonucleotides. Mutation research. 823:58–64. [PubMed: 28985947]

DeJesus OT. 2017. Chemical Consequences of Radioactive Decay and their Biological Implications. Current radiopharmaceuticals. 10(3):155–165. [PubMed: 28714401]

Delorme R, Taupin F, Flaender M, Ravanat JL, Champion C, Agelou M, Elleaume H. 2017. Comparison of gadolinium nanoparticles and molecular contrast agents for radiation therapy-enhancement. Med Phys. 44(11):5949–5960. [PubMed: 28886212]

Di Maria S, Belchior A, Romanets Y, Paulo A, Vaz P. 2018. Monte Carlo dose distribution calculation at nuclear level for Auger-emitting radionuclide energies. Applied radiation and isotopes : including data, instrumentation and methods for use in agriculture, industry and medicine. 135:72–77. [PubMed: 29413839]

Dong S, Pal S, Lian J, Chan Y, Prezhdo OV, Loh ZH. 2016. Sub-Picosecond Auger-Mediated Hole-Trapping Dynamics in Colloidal CdSe/CdS Core/Shell Nanoplatelets. ACS nano. 10(10):9370–9378. [PubMed: 27640430]

Duchemin C, Guertin A, Haddad F, Michel N, Metivier V. 2016. Deuteron induced Tb-155 production, a theranostic isotope for SPECT imaging and auger therapy. Applied radiation and isotopes : including data, instrumentation and methods for use in agriculture, industry and medicine. 118:281–289. [PubMed: 27723559]

Eckerman KF, Endo A. 2008. MIRD: Radionuclide Data and Decay Schemes. 2nd ed. Reston, VA: Society of Nuclear Medicine.

Ertl HH, Feinendegen LE, Heiniger HJ. 1970. Iodine-125, a tracer in cell biology: Physical properties and biological aspects. Phys Med Biol. 15:447–456. [PubMed: 5485455]

Fairchild RG, Bond VP. 1984. Photon activation therapy. Strahlentherapie. 160:758–763. [PubMed: 6515666]

Falzone N, Lee BQ, Able S, Malcolm J, Terry S, Alayed Y, Vallis KA. 2018. Targeting Micrometastases: The Effect of Heterogeneous Radionuclide Distribution on Tumor Control Probability. J Nucl Med. 60:250–258. [PubMed: 29959216]

Falzone N, Lee BQ, Able S, Malcolm J, Terry S, Alayed Y, Vallis KA. 2019. Targeting Micrometastases: The Effect of Heterogeneous Radionuclide Distribution on Tumor Control Probability. Journal of nuclear medicine : official publication, Society of Nuclear Medicine. 60:250–258.

Falzone N, Lee BQ, Fernandez-Varea JM, Kartsonaki C, Stuchbery AE, Kibedi T, Vallis KA. 2017. Absorbed dose evaluation of Auger electron-emitting radionuclides: impact of input decay spectra on dose point kernels and S-values. Physics in medicine and biology. 62(6):2239–2253. [PubMed: 28102829]

Fasshauer E, Kolorenc P, Pernpointner M. 2015. Relativistic decay widths of autoionization processes: the relativistic FanoADC-Stieltjes method. The Journal of chemical physics. 142(14):144106. [PubMed: 25877561]

Feifel R, Eland JH, Squibb RJ, Mucke M, Zagorodskikh S, Linusson P, Tarantelli F, Kolorenc P, Averbukh V. 2016. Ultrafast Molecular Three-Electron Auger Decay. Physical review letters. 116(7):073001. [PubMed: 26943531]

Feinendegen LE. 1975. Biological damage from the Auger effect, possible benefits. Radiat Environ Biophys. 12:85–99. [PubMed: 1101289]

Ferreira N, Sigaud L, Montenegro EC. 2017. Three-Body Fragmentation from Single Ionization of Water by Electron Impact: The Role of Satellite States. The journal of physical chemistry A. 121(17):3234–3238. [PubMed: 28407714]

Fonslet J, Lee BQ, Tran TA, Siragusa M, Jensen M, Kibedi T, Stuchbery AE, Severin GW. 2017. ^{135}La as an Auger-electron emitter for targeted internal radiotherapy. Physics in medicine and biology. 63(1):015026. [PubMed: 29286003]

Fourie H, Newman RT, Slabbert JP. 2015. Microdosimetry of the Auger electron emitting 123I radionuclide using Geant4-DNA simulations. Phys Med Biol. 60(8):3333–3346. [PubMed: 25825914]

Frolova LV, Magedov IV, Harper A, Jha SK, Ovezmyradov M, Chandler G, Garcia J, Bethke D, Shaner EA, Vasiliev I et al. 2015. Tetracyanoethylene oxide- functionalized graphene and graphite characterized by Raman and Auger spectroscopy. Carbon. 81:216–222. [PubMed: 25484371]

Fukunaga H, Kaminaga K, Sato T, Usami N, Watanabe R, Butterworth KT, Ogawa T, Yokoya A, Prise KM. 2018. Application of an Ex Vivo Tissue Model to Investigate Radiobiological Effects on Spermatogenesis. Radiat Res. 189(6):661–667. [PubMed: 29595376]

Fukuzawa H, Takanashi T, Kukk E, Motomura K, Wada SI, Nagaya K, Ito Y, Nishiyama T, Nicolas C, Kumagai Y et al. 2019. Real-time observation of X-ray-induced intramolecular and interatomic electronic decay in CH2I2. Nature communications. 10(1):2186.

Gao C, Leyton JV, Schimmer AD, Minden M, Reilly RM. 2016. Auger electron-emitting 111In-DTPA-NLS-CSL360 radioimmunoconjugates are cytotoxic to human acute myeloid leukemia (AML) cells displaying the CD123^{+}/CD131^{-} phenotype of leukemia stem cells. Applied radiation and isotopes : including data, instrumentation and methods for use in agriculture, industry and medicine. 110:1–7. [PubMed: 26748017]

Gessner O, Guhr M. 2016. Monitoring Ultrafast Chemical Dynamics by Time-Domain X-ray Photo- and Auger-Electron Spectroscopy. Accounts of chemical research. 49(1):138–145. [PubMed: 26641490]

Ghirmai S, Mume E, Tolmachev V, Sjoberg S. 2005. Synthesis and radioiodination of some daunorubicin and doxorubicin derivatives. Carbohydrate research. 340(1):15–24. eng. [PubMed: 15620662]

Ghosh A, Pal S, Vaval N. 2015. Lifetime of inner-shell hole states of Ar (2p) and Kr (3d) using equation-of-motion coupled cluster method. The Journal of chemical physics. 143(2):024305. [PubMed: 26178103]

Gierz I, Calegari F, Aeschlimann S, Chavez Cervantes M, Cacho C, Chapman RT, Springate E, Link S, Starke U, Ast CR et al. 2015. Tracking Primary Thermalization Events in Graphene with Photoemission at Extreme Time Scales. Physical review letters. 115(8):086803. [PubMed: 26340199]

Gill MR, Falzone N, Du Y, Vallis KA. 2017. Targeted radionuclide therapy in combined-modality regimens. The Lancet Oncology. 18(7):e414–e423. [PubMed: 28677577]

Gill MR, Menon JU, Jarman PJ, Owen J, Skaripa-Koukelli I, Able S, Thomas JA, Carlisle R, Vallis KA. 2018. ^{111}In-labelled polymeric nanoparticles incorporating a ruthenium-based radiosensitizer for EGFR-targeted combination therapy in oesophageal cancer cells. Nanoscale. 10(22):10596–10608. [PubMed: 29808844]

Gill MR, Vallis KA. 2019. Transition metal compounds as cancer radiosensitizers. Chemical Society reviews. 48(2):540–557. [PubMed: 30499573]

Giovanni D, Yu G, Xing G, Leek ML, Sum TC. 2015. Measurement of sub-10 fs Auger processes in monolayer graphene. Optics express. 23(16):21107–21117. [PubMed: 26367961]

Giussani A 2015. Models and phantoms for internal dose assessment. Radiat Prot Dosimetry. 164(1–2):46–50. [PubMed: 25305216]

Goddu SM, Howell RW, Bouchet LG, Bolch WE, Rao DV. 1997. MIRD Cellular S values: self-absorbed dose per unit cumulated activity for selected radionuclides and monoenergetic electron and alpha particle emitters incorporated into different cell compartments. Reston, VA: Society of Nuclear Medicine.

Goddu SM, Howell RW, Rao DV. 1994. Cellular dosimetry: absorbed fractions for monoenergetic electron and alpha particle sources and S-values for radionuclides uniformly distributed in different cell compartments. J Nucl Med. 35(2):303–316. [PubMed: 8295004]

Goddu SM, Narra VR, Harapanhalli RS, Howell RW, Rao DV. 1996. Radioprotection by DMSO against the biological effects of incorporated radionuclides *in vivo*. Acta oncologica. 35(7):901–907. [PubMed: 9004770]

Goldsztejn G, Marchenko T, Ceolin D, Journel L, Guillemin R, Rueff JP, Kushawaha RK, Puttner R, Piancastelli MN, Simon M. 2016. Electronic state-lifetime interference in resonant Auger spectra: a tool to disentangle overlapping core-excited states. Physical chemistry chemical physics : PCCP. 18(22):15133–15142. [PubMed: 27199185]

Goldsztejn G, Marchenko T, Puttner R, Journel L, Guillemin R, Carniato S, Selles P, Travnikova O, Ceolin D, Lago AF et al. 2016. Double-Core-Hole States in Neon: Lifetime, Post-Collision Interaction, and Spectral Assignment. Physical review letters. 117(13):133001. [PubMed: 27715102]

Gorobtsov OY, Lorenz U, Kabachnik NM, Vartanyants IA. 2015. Theoretical study of electronic damage in single-particle imaging experiments at x-ray free-electron lasers for pulse durations from 0.1 to 10 fs. Physical review E, Statistical, nonlinear, and soft matter physics. 91(6):062712. [PubMed: 26172741]

Grokhovsky SL. 2018. [Use of beta Radiation to Localize the Binding Sites of Mercury Ions and Platinum-Containing Ligand in DNA]. Molekuliarnaia biologiia. 52(5):846–863. [PubMed: 30363060]

Grudzinski J, Marsh I, Titz B, Jeffery J, Longino M, Kozak K, Lange K, Larrabee J, Weichmann A, Moser A et al. 2018. CLR 125 Auger Electrons for the Targeted Radiotherapy of Triple-Negative Breast Cancer. Cancer Biother Radiopharm. 33(3):87–95. [PubMed: 29641256]

Gudkov SV, Shilyagina NY, Vodeneev VA, Zvyagin AV. 2015. Targeted Radionuclide Therapy of Human Tumors. International journal of molecular sciences. 17(1).

Guerra Liberal FDC, Tavares AAS, Tavares J. 2016. Palliative treatment of metastatic bone pain with radiopharmaceuticals: A perspective beyond Strontium-89 and Samarium-153. Applied radiation and isotopes : including data, instrumentation and methods for use in agriculture, industry and medicine. 110:87–99. [PubMed: 26773820]

Guerreiro JF, Alves V, Abrunhosa AJ, Paulo A, Gil OM, Mendes F. 2018. Radiobiological Characterization of $^{64}CuCl_2$ as a Simple Tool for Prostate Cancer Theranostics. Molecules. 23(11).

Haefliger P, Agorastos N, Renard A, Giambonini-Brugnoli G, Marty C, Alberto R. 2005. Cell uptake and radiotoxicity studies of an nuclear localization signal peptide-intercalator conjugate labeled with [$^{99m}Tc(CO)3$]+. Bioconjugate chemistry. 16(3):582–587. eng. [PubMed: 15898725]

Hafliger P, Agorastos N, Spingler B, Georgiev O, Viola G, Alberto R. 2005. Induction of DNA-double-strand breaks by auger electrons from ^{99m}Tc complexes with DNA-binding ligands. Chembiochem. 6(2):414–421. [PubMed: 15651047]

Haller S, Pellegrini G, Vermeulen C, van der Meulen NP, Koster U, Bernhardt P, Schibli R, Muller C. 2016. Contribution of Auger/conversion electrons to renal side effects after radionuclide therapy: preclinical comparison of ^{161}Tb-folate and ^{177}Lu-folate. EJNMMI research. 6(1):13. [PubMed: 26860295]

Hans A, Ozga C, Seidel R, Schmidt P, Ueltzhoffer T, Holzapfel X, Wenzel P, Reiss P, Pohl MN, Unger I et al. 2017. Optical Fluorescence Detected from X-ray Irradiated Liquid Water. The journal of physical chemistry B. 121(10):2326–2330. [PubMed: 28187257]

Harapanhalli RS, Narra VR, Yaghmai V, Azure MT, Goddu SM, Howell RW, Rao DV. 1994. Vitamins as radioprotectors in vivo. II. Protection by vitamin A and soybean oil against radiation damage caused by internal radionuclides. Radiat Res. 139:115–122. [PubMed: 8016300]

He SJ, Wang DK, Jiang N, Tse JS, Lu ZH. 2016. Tunable Excitonic Processes at Organic Heterojunctions. Advanced materials. 28(4):649–654. [PubMed: 26797983]

Herve du Penhoat MA, Ghose KK, Gaigeot MP, Vuilleumier R, Fujii K, Yokoya A, Politis MF. 2015. Investigation of the fragmentation of core-ionised deoxyribose: a study as a function of the

tautomeric form. Physical chemistry chemical physics : PCCP. 17(48):32375–32383. [PubMed: 26584628]

Heuskin AC, Gallez B, Feron O, Martinive P, Michiels C, Lucas S. 2017. Metallic nanoparticles irradiated by low-energy protons for radiation therapy: Are there significant physical effects to enhance the dose delivery? Med Phys. 44(8):4299–4312. [PubMed: 28543610]

Hindie E, Zanotti-Fregonara P, Quinto MA, Morgat C, Champion C. 2016. Dose Deposits from 90Y, 177Lu, 111In, and 161Tb in Micrometastases of Various Sizes: Implications for Radiopharmaceutical Therapy. J Nucl Med. 57(5):759–764. [PubMed: 26912441]

Hofer KG. 1992. Closing address: Biophysical aspects of Auger processes. In: Howell RW, Narra VR, Sastry KSR et al., editors. Biophysical Aspects of Auger Processes. Woodbury, NY: American Institute of Physics (http://www.aapm.org/pubs/books/PROC_8.pdf); p. 403–412.

Hofer KG. 1996. Biophysical aspects of Auger processes--A review. Acta oncologica. 35(7):789–796. eng. [PubMed: 9004754]

Hofer KG. 2000. Biophysical aspects of Auger processes. Acta oncologica. 39(6):651–657. [PubMed: 11130000]

Hofer KG, Hughes WL. 1971. Radiotoxicity of intranuclear tritium, iodine-125 and iodine-131. Radiat Res. 47:94–109. [PubMed: 5559387]

Hou DY, Hoch H, Johnston GS, Tsou KC, Jones AE, Farkas RJ, Miller EE, Larson SM. 1985. A new In-111 bleomycin complex for combined radiotherapy and chemotherapy. Journal of Surgical Oncology. 29:91–98. [PubMed: 2417055]

Howell RW. 1992. Radiation spectra for Auger-electron emitting radionuclides: Report No. 2 of AAPM Nuclear Medicine Task Group No. 6. Med Phys. 19(6):1371–1383. [PubMed: 1461199]

Howell RW. 2008. Auger processes in the 21st century. International journal of radiation biology. 84(12):959–975. eng. [PubMed: 19061120]

Howell RW, Bishayee A. 2002. Bystander effects caused by nonuniform distributions of DNA-incorporated ^{125}I. Micron. 33:127–132. [PubMed: 11567881]

Howell RW, Kassis AI, Adelstein SJ, Rao DV, Wright HA, Hamm RN, Turner JE, Sastry KSR. 1994. Radiotoxicity of ^{195m}Pt labeled trans-platinum(II) in mammalian cells. Radiat Res. 140:55–62. [PubMed: 7938455]

Howell RW, Narra VR, Rao DV, Sastry KSR. 1990. Radiobiological effects of intracellular polonium-210 alpha emissions: A comparison with Auger-emitters. Radiat Prot Dosim. 31:325–328.

Howell RW, Narra VR, Sastry KSR, Rao DV, editors. 1992. Biophysical Aspects of Auger Processes. New York: American Institute of Physics (http://www.aapm.org/pubs/books/PROC_8.pdf). (AAPM Symposium Proceedings No 8.

Howell RW, Rao DV. 2002. In Memoriam: Prof. Kandula S.R. Sastry 1935–2001. J Nucl Med. 43(1):12N.

Howell RW, Rao DV, Hou D-Y, Narra VR, Sastry KSR. 1991. The question of relative biological effectiveness and quality factor for Auger emitters incorporated into proliferating mammalian cells. Radiat Res. 128:282–292. [PubMed: 1961925]

Howell RW, Rao DV, Sastry KSR. 1989. Macroscopic dosimetry for radioimmunotherapy: nonuniform activity distributions in solid tumors. Med Phys. 16:66–74. [PubMed: 2921982]

Howell RW, Sastry KSR, Hill HZ, Rao DV. 1986. Cis-platinum-193m: Its microdosimetry and potential for chemo-Auger combination therapy of cancer. In: Schlafke-Stelson AT, Watson EE, editors. Proceedings of Fourth International Radiopharmaceutical Dosimetry Symposium. Springfield, VA: National Technical Information Service; p. 493–513.

Hult Roos A, Eland JHD, Andersson J, Wallner M, Squibb RJ, Feifel R. 2019. Relative extent of triple Auger decay in CO and CO2. Physical chemistry chemical physics : PCCP. 21(19):9889–9894. [PubMed: 31038513]

Humm JL, Nikjoo H. 2013. David E. Charlton (1936–2013). Radiat Res. 180(5):553–555. [PubMed: 24245658]

Iablonskyi D, Nagaya K, Fukuzawa H, Motomura K, Kumagai Y, Mondal S, Tachibana T, Takanashi T, Nishiyama T, Matsunami K et al. 2016. Slow Interatomic Coulombic Decay of Multiply Excited Neon Clusters. Physical review letters. 117(27):276806. [PubMed: 28084773]

Iablonskyi D, Ueda K, Ishikawa KL, Kheifets AS, Carpeggiani P, Reduzzi M, Ahmadi H, Comby A, Sansone G, Csizmadia T et al. 2017. Observation and Control of Laser-Enabled Auger Decay. Physical review letters. 119(7):073203. [PubMed: 28949652]

Ickenstein LM, Edwards K, Sjoberg S, Carlsson J, Gedda L. 2006. A novel ^{125}I-labeled daunorubicin derivative for radionuclide-based cancer therapy. Nucl Med Biol. 33(6):773–783. eng. [PubMed: 16934696]

ICRP. 2007. Publication 103: The 2007 Recommendations of the International Commission on Radiological Protection. Annals of the ICRP. 37:1–332.

ICRU. 2011. ICRU Report No. 86. Quantification and reporting of low-dose and other heterogeneous exposures. Journal of the ICRU. 11(2):1–77.

Imstepf S, Pierroz V, Raposinho P, Bauwens M, Felber M, Fox T, Shapiro AB, Freudenberg R, Fernandes C, Gama S et al. 2015. Nuclear Targeting with an Auger Electron Emitter Potentiates the Action of a Widely Used Antineoplastic Drug. Bioconjugate chemistry. 26(12):2397–2407. [PubMed: 26473388]

Iskandar W, Matsumoto J, Leredde A, Flechard X, Gervais B, Guillous S, Hennecart D, Mery A, Rangama J, Zhou CL et al. 2015. Interatomic Coulombic decay as a new source of low energy electrons in slow ion-dimer collisions. Physical review letters. 114(3):033201. [PubMed: 25658997]

Iwayama H, Kaneyasu T, Hikosaka Y, Shigemasa E. 2016. Stability and dissociation dynamics of N2 (++) ions following core ionization studied by an Auger-electron-photoion coincidence method. The Journal of chemical physics. 145(3):034305. [PubMed: 27448885]

Jaaskela-Saari HA, Grenman R, Ramsay HA, Tarkkanen J, Paavonen T, Kairemo KJ. 2005. Indium-111-bleomycin complex in squamous cell cancer xenograft tumors of nude mice. Cancer biotherapy & radiopharmaceuticals. 20(4):426–435. eng. [PubMed: 16114991]

Jablonski A, Powell CJ. 2017. Effective attenuation lengths for quantitative determination of surface composition by Auger-electron spectroscopy and X-ray photoelectron spectroscopy. Journal of electron spectroscopy and related phenomena. 281:1–2. [PubMed: 29249851]

Jeon JK, Han SM, Kim JK. 2016. Fluorescence imaging of reactive oxygen species by confocal laser scanning microscopy for track analysis of synchrotron X-ray photoelectric nanoradiator dose: X-ray pump-optical probe. Journal of synchrotron radiation. 23(Pt 5):1191–1196. [PubMed: 27577774]

Kai T, Yokoya A, Ukai M, Fujii K, Toigawa T, Watanabe R. 2018. A significant role of non-thermal equilibrated electrons in the formation of deleterious complex DNA damage. Physical chemistry chemical physics : PCCP. 20(4):2838–2844. [PubMed: 29327017]

Kai T, Yokoya A, Ukai M, Fujii K, Watanabe R. 2016a. Deceleration processes of secondary electrons produced by a high-energy Auger electron in a biological context. Int J Radiat Biol. 92(11):654–659. [PubMed: 27332896]

Kai T, Yokoya A, Ukai M, Fujii K, Watanabe R. 2016b. Dynamic Behavior of Secondary Electrons in Liquid Water at the Earliest Stage upon Irradiation: Implications for DNA Damage Localization Mechanism. The journal of physical chemistry A. 120(42):8228–8233. [PubMed: 27690437]

Kaminaga K, Noguchi M, Narita A, Hattori Y, Usami N, Yokoya A. 2016. Cell cycle tracking for irradiated and unirradiated bystander cells in a single colony with exposure to a soft X-ray microbeam. Int J Radiat Biol. 92(11):739–744. [PubMed: 27537347]

Kaneyasu T, Odagiri T, Nakagawa M, Mashiko R, Tanaka H, Adachi J, Hikosaka Y. 2017. Single, double, and triple Auger decays from 1s shake-up states of the oxygen molecule. The Journal of chemical physics. 147(10):104304. [PubMed: 28915746]

Kassis AI. 2004. The amazing world of Auger electrons. Int J Radiat Biol. 80(11–12):789–803. [PubMed: 15764386]

Kassis AI, Adelstein SJ, Haydock C, Sastry KSR, McElvany KD, Welch MJ. 1982. Lethality of Auger electrons from the decay of bromine-77 in the DNA of mammalian cells. Radiat Res. 90:362–373. [PubMed: 7079468]

Kassis AI, Fayad F, Kinsey BM, Sastry KSR, Taube RA, Adelstein SJ. 1987. Radiotoxicity of I-125 in mammalian cells. Radiat Res. 111:305–318. [PubMed: 3628718]

Kelbg M, Zabel M, Krebs B, Kazak L, Meiwes-Broer KH, Tiggesbaumker J. 2019. Auger emission from the Coulomb explosion of helium nanoplasmas. The Journal of chemical physics. 150(20):204302. [PubMed: 31153176]

Kiess AP, Minn I, Chen Y, Hobbs R, Sgouros G, Mease RC, Pullambhatla M, Shen CJ, Foss CA, Pomper MG. 2015. Auger Radiopharmaceutical Therapy Targeting Prostate-Specific Membrane Antigen. J Nucl Med. 56(9):1401–1407. [PubMed: 26182968]

Kirkland JL, Tchkonia T, Zhu Y, Niedernhofer LJ, Robbins PD. 2017. The Clinical Potential of Senolytic Drugs. Journal of the American Geriatrics Society. 65(10):2297–2301. [PubMed: 28869295]

Kojima T, Aihara H, Kodashima Y, Makishima H, Nakiri S, Takada S, Shimada H, Ukai M, Ozga C, Holzapfel X et al. 2019. Novel Analytical Study for Reaction Intermediates in the Primary Radiation Interaction of DNA Using a Synchrotron Radiation-Induced Luminescence Spectroscopy. Radiat Prot Dosimetry. 183(1–2):32–35. [PubMed: 30753692]

Kortylewicz ZP, Mack E, Enke CA, Estes KA, Mosley RL, Baranowska-Kortylewicz J. 2015. Preclinical evaluation of investigational radiopharmaceutical RISAD-P intended for use as a diagnostic and molecular radiotherapy agent for prostate cancer. The Prostate. 75(1):8–22. [PubMed: 25283970]

Kotzerke J, Runge R, Gotze P, Wunderlich G, Enghardt W, Freudenberg R. 2019. [Radio- and photosensitization of plasmid DNA by DNA binding ligand propidium iodide: Investigation of Auger electron induction and detection of Cherenkov-emission]. Nuklearmedizin Nuclear medicine.

Ku A, Facca VJ, Cai Z, Reilly RM. 2019. Auger electrons for cancer therapy - a review. EJNMMI radiopharmacy and chemistry. 4(1):27. [PubMed: 31659527]

Kuleff AI, Kryzhevoi NV, Pernpointner M, Cederbaum LS. 2016. Core Ionization Initiates Subfemtosecond Charge Migration in the Valence Shell of Molecules. Physical review letters. 117(9):093002. [PubMed: 27610850]

Kumar SV, Tare ST, Upalekar YV, Tsering T. 2016. Dose controlled low energy electron irradiator for biomolecular films. The Review of scientific instruments. 87(3):034302. [PubMed: 27036792]

Ladjohounlou R, Lozza C, Pichard A, Constanzo J, Karam J, Le Fur P, Deshayes E, Boudousq V, Paillas S, Busson M et al. 2019. Drugs That Modify Cholesterol Metabolism Alter the p38/JNK-Mediated Targeted and Nontargeted Response to Alpha and Auger Radioimmunotherapy. Clin Cancer Res.

Lechtman E, Pignol JP. 2017. Interplay between the gold nanoparticle sub-cellular localization, size, and the photon energy for radiosensitization. Scientific reports. 7(1):13268. [PubMed: 29038517]

Lee BQ, Nikjoo H, Ekman J, Jonsson P, Stuchbery AE, Kibedi T. 2016. A stochastic cascade model for Auger-electron emitting radionuclides. Int J Radiat Biol. 92(11):641–653. [PubMed: 27010453]

Lee D, Li M, Bednarz B, Schultz MK. 2018. Modeling Cell and Tumor-Metastasis Dosimetry with the Particle and Heavy Ion Transport Code System (PHITS) Software for Targeted Alpha-Particle Radionuclide Therapy. Radiation research. 190(3):236–247. [PubMed: 29944461]

Leung CN, Canter BS, Rajon D, Back TA, Fritton JC, Azzam EI, Howell RW. 2020. Dose-Dependent Growth Delay of Breast Cancer Xenografts in the Bone Marrow of Mice Treated with Radium-223: The Role of Bystander Effects and their Potential for Therapy. J Nucl Med. 61(1):89–95. [PubMed: 31519805]

Leyton JV, Gao C, Williams B, Keating A, Minden M, Reilly RM. 2015. A radiolabeled antibody targeting CD123^{+} leukemia stem cells - initial radioimmunotherapy studies in NOD/SCID mice engrafted with primary human AML. Leukemia research reports. 4(2):55–59. [PubMed: 26500848]

Li HK, Morokoshi Y, Daino K, Furukawa T, Kamada T, Saga T, Hasegawa S. 2015. Transcriptomic Signatures of Auger Electron Radioimmunotherapy Using Nuclear Targeting ^{111}In-Trastuzumab for Potential Combination Therapies. Cancer biotherapy & radiopharmaceuticals. 30(8):349–358. [PubMed: 26447839]

Li L, Jaraquemada-Pelaez MG, Kuo HT, Merkens H, Choudhary N, Gitschtaler K, Jermilova U, Colpo N, Uribe-Munoz C, Radchenko V et al. 2019. Functionally Versatile and Highly Stable

Chelator for ^{111}In and [177]Lu: Proof-of-Principle Prostate-Specific Membrane Antigen Targeting. Bioconjugate chemistry. 30(5):1539–1553. [PubMed: 31009566]

Li Z, Vendrell O, Santra R. 2015. Ultrafast Charge Transfer of a Valence Double Hole in Glycine Driven Exclusively by Nuclear Motion. Physical review letters. 115(14):143002. [PubMed: 26551809]

Liekhus-Schmaltz CE, Tenney I, Osipov T, Sanchez-Gonzalez A, Berrah N, Boll R, Bomme C, Bostedt C, Bozek JD, Carron S et al. 2015. Ultrafast isomerization initiated by X-ray core ionization. Nature communications. 6:8199.

Liko F, Hindre F, Fernandez-Megia E. 2016. Dendrimers as Innovative Radiopharmaceuticals in Cancer Radionanotherapy. Biomacromolecules. 17(10):3103–3114. [PubMed: 27608327]

Liu P, Boyle AJ, Lu Y, Adams J, Chi Y, Reilly RM, Winnik MA. 2015. Metal-Chelating Polymers (MCPs) with Zwitterionic Pendant Groups Complexed to Trastuzumab Exhibit Decreased Liver Accumulation Compared to Polyanionic MCP Immunoconjugates. Biomacromolecules. 16(11):3613–3623. [PubMed: 26469142]

Liu XJ, Nicolas C, Patanen M, Miron C. 2017. Disentangling Auger decays in O2 by photoelectron-ion coincidences. Scientific reports. 7(1):2898. [PubMed: 28588192]

Lobachevsky P, Clark GR, Pytel PD, Leung B, Skene C, Andrau L, White JM, Karagiannis T, Cullinane C, Lee BQ et al. 2016. Strand breakage by decay of DNA-bound [124]I provides a basis for combined PET imaging and Auger endoradiotherapy. International journal of radiation biology. 92(11):686–697. [PubMed: 26902391]

Makrigiorgos GM, Kassis AI, Baranowska-Kortylewicz J, McElvany KD, Welch MJ, Sastry KSR, Adelstein SJ. 1989. Radiotoxicity of 5-[^{123}I]iodo-2'-deoxyuridine in V79 cells: a comparison with 5-[^{125}I]iodo-2'-deoxyuridine. Radiat Res. 118:532–544. [PubMed: 2727274]

Martin RF, Feinendegen LE. 2016. The quest to exploit the Auger effect in cancer radiotherapy - a reflective review. International journal of radiation biology. 92(11):617–632. [PubMed: 26926313]

Martinez-Rovira I, Prezado Y. 2015. Evaluation of the local dose enhancement in the combination of proton therapy and nanoparticles. Med Phys. 42(11):6703–6710. [PubMed: 26520760]

Martins CD, Kramer-Marek G, Oyen WJG. 2018. Radioimmunotherapy for delivery of cytotoxic radioisotopes: current status and challenges. Expert opinion on drug delivery. 15(2):185–196. [PubMed: 28893110]

Maucksch U, Runge R, Oehme L, Kotzerke J, Freudenberg R. 2018. Radiotoxicity of alpha particles versus high and low energy electrons in hypoxic cancer cells. Nuklearmedizin Nuclear medicine. 57(2):56–63. [PubMed: 29590676]

Maucksch U, Runge R, Wunderlich G, Freudenberg R, Naumann A, Kotzerke J. 2016. Comparison of the radiotoxicity of the ^{99m}Tc-labeled compounds ^{99m}Tc-pertechnetate, ^{99m}Tc-HMPAO and ^{99m}Tc-MIBI. International journal of radiation biology. 92(11):698–706. [PubMed: 27117205]

McMahon SJ, Paganetti H, Prise KM. 2016. Optimising element choice for nanoparticle radiosensitisers. Nanoscale. 8(1):581–589. [PubMed: 26645621]

McMillan DD, Maeda J, Bell JJ, Genet MD, Phoonswadi G, Mann KA, Kraft SL, Kitamura H, Fujimori A, Yoshii Y et al. 2015. Validation of 64Cu-ATSM damaging DNA via high-LET Auger electron emission. Journal of radiation research (Tokyo). 56(5):784–791.

McNamara AL, Kam WW, Scales N, McMahon SJ, Bennett JW, Byrne HL, Schuemann J, Paganetti H, Banati R, Kuncic Z. 2016. Dose enhancement effects to the nucleus and mitochondria from gold nanoparticles in the cytosol. Phys Med Biol. 61(16):5993–6010. [PubMed: 27435339]

Meitner L 1923. Das β-strahlenspektrum von UX₁ und seine deutung. Zeitschrift für Physik. 17:54–66.

Mikell J, Cheenu Kappadath S, Wareing T, Erwin WD, Titt U, Mourtada F. 2016. Evaluation of a deterministic grid-based Boltzmann solver (GBBS) for voxel-level absorbed dose calculations in nuclear medicine. Phys Med Biol. 61(12):4564–4582. [PubMed: 27224727]

Miran T, Vogg ATJ, Drude N, Mottaghy FM, Morgenroth A. 2018. Modulation of glutathione promotes apoptosis in triple-negative breast cancer cells. FASEB journal : official publication of the Federation of American Societies for Experimental Biology. 32(5):2803–2813. [PubMed: 29301945]

Miran T, Vogg ATJ, El Moussaoui L, Kaiser HJ, Drude N, von Felbert V, Mottaghy FM, Morgenroth A. 2017. Dual addressing of thymidine synthesis pathways for effective targeting of proliferating melanoma. Cancer medicine. 6(7):1639–1651. [PubMed: 28608446]

Miteva T, Kazandjian S, Kolorenc P, Votavova P, Sisourat N. 2017. Interatomic Coulombic Decay Mediated by Ultrafast Superexchange Energy Transfer. Physical review letters. 119(8):083403. [PubMed: 28952742]

Moser F, Hildenbrand G, Muller P, Al Saroori A, Biswas A, Bach M, Wenz F, Cremer C, Burger N, Veldwijk MR et al. 2016. Cellular Uptake of Gold Nanoparticles and Their Behavior as Labels for Localization Microscopy. Biophysical journal. 110(4):947–953. [PubMed: 26910431]

Mukherjee S, Shastry K, Anto CV, Joglekar PV, Nadesalingam MP, Xie S, Jiang N, Weiss AH. 2016. Time of flight spectrometer for background-free positron annihilation induced Auger electron spectroscopy. The Review of scientific instruments. 87(3):035114. [PubMed: 27036826]

Muller A, Borovik A Jr., Buhr T, Hellhund J, Holste K, Kilcoyne AL, Klumpp S, Martins M, Ricz S, Viefhaus J et al. 2015. Observation of a four-electron Auger process in near-K-edge photoionization of singly charged carbon ions. Physical review letters. 114(1):013002. [PubMed: 25615465]

Muller C, Domnanich KA, Umbricht CA, van der Meulen NP. 2018. Scandium and terbium radionuclides for radiotheranostics: current state of development towards clinical application. Br J Radiol. 91(1091):20180074. [PubMed: 29658792]

Muller C, Umbricht CA, Gracheva N, Tschan VJ, Pellegrini G, Bernhardt P, Zeevaart JR, Koster U, Schibli R, van der Meulen NP. 2019. Terbium-161 for PSMA-targeted radionuclide therapy of prostate cancer. Eur J Nucl Med Mol Imaging.

Muller C, van der Meulen NP, Benesova M, Schibli R. 2017. Therapeutic Radiometals Beyond (177)Lu and (90)Y: Production and Application of Promising alpha-Particle, beta(−)-Particle, and Auger Electron Emitters. J Nucl Med. 58(Suppl 2):91S–96S. [PubMed: 28864619]

Murray PJ, Cornelissen B, Vallis KA, Chapman SJ. 2016. DNA double-strand break repair: a theoretical framework and its application. Journal of the Royal Society, Interface. 13(114):20150679. [PubMed: 26819332]

Nagaya K, Iablonskyi D, Golubev NV, Matsunami K, Fukuzawa H, Motomura K, Nishiyama T, Sakai T, Tachibana T, Mondal S et al. 2016. Interatomic Coulombic decay cascades in multiply excited neon clusters. Nature communications. 7:13477.

Nagaya K, Motomura K, Kukk E, Takahashi Y, Yamazaki K, Ohmura S, Fukuzawa H, Wada S, Mondal S, Tachibana T et al. 2016. Femtosecond charge and molecular dynamics of I-containing organic molecules induced by intense X-ray free-electron laser pulses. Faraday discussions. 194:537–562. [PubMed: 27797386]

Narra VR, Harapanhalli RS, Howell RW, Sastry KSR, Rao DV. 1992. Chemical protection against radionuclides in vivo: Implications to the mechanism of the Auger effect. In: Howell RW, Narra VR, Sastry KSR et al., editors. Biophysical Aspects of Auger Processes. Woodbury, NY: AmerAmerican Institute of Physics (http://www.aapm.org/pubs/books/PROC_8.pdf); p. 319–335.

Neti PV, Howell RW. 2006. Log normal distribution of cellular uptake of radioactivity: implications for biologic responses to radiopharmaceuticals. J Nucl Med. 47(6):1049–1058. eng. [PubMed: 16741316]

Nettleton JS, Lawson R. 1996. Cellular dosimetry of diagnostic radionuclides for spherical and ellipsoidal geometry. Phys Med Biol. 41(9):1845–1854. [PubMed: 8884915]

Ngo Ndjock Mbong G, Lu Y, Chan C, Cai Z, Liu P, Boyle AJ, Winnik MA, Reilly RM. 2015. Trastuzumab Labeled to High Specific Activity with ^{111}In by Site-Specific Conjugation to a Metal-Chelating Polymer Exhibits Amplified Auger Electron-Mediated Cytotoxicity on HER2-Positive Breast Cancer Cells. Molecular pharmaceutics. 12(6):1951–1960. [PubMed: 25919639]

Nicolas GP, Mansi R, McDougall L, Kaufmann J, Bouterfa H, Wild D, Fani M. 2017. Biodistribution, Pharmacokinetics, and Dosimetry of [177]Lu-, [90]Y-, and ^{111}In-Labeled Somatostatin Receptor Antagonist OPS201 in Comparison to the Agonist ^{177}Lu-DOTATATE: The Mass Effect. Journal of nuclear medicine : official publication, Society of Nuclear Medicine. 58(9):1435–1441. [PubMed: 28450554]

Nicolas GP, Morgenstern A, Schottelius M, Fani M. 2018. New Developments in Peptide Receptor Radionuclide Therapy. J Nucl Med.

Nikjoo H, Girard P, Charlton DE, Hofer KG, Laughton CA. 2006. Auger electrons--a nanoprobe for structural, molecular and cellular processes. Radiat Prot Dosim. 122:72–79. Eng.

Oehme L, Bartzsch T, Maucksch U, Freudenberg R, Wunderlich G, Kotzerke J. 2018. [Combined internal-external radiotherapy (CIERT) in a cell model]. Nuklearmedizin Nuclear medicine. 57(3):108–116. [PubMed: 29871012]

Othman MF, Mitry NR, Lewington VJ, Blower PJ, Terry SY. 2017. Re-assessing gallium-67 as a therapeutic radionuclide. Nucl Med Biol. 46:12–18. [PubMed: 27915165]

Paillas S, Boudousq V, Piron B, Kersual N, Bardies M, Chouin N, Bascoul-Mollevi C, Arnaud FX, Pelegrin A, Navarro-Teulon I et al. 2013. Apoptosis and p53 are not involved in the antitumor efficacy of (1)(2)(5)I-labeled monoclonal antibodies targeting the cell membrane. Nucl Med Biol. 40(4):471–480. [PubMed: 23522976]

Paillas S, Ladjohounlou R, Lozza C, Pichard A, Boudousq V, Jarlier M, Sevestre S, Le Blay M, Deshayes E, Sosabowski J et al. 2016. Localized Irradiation of Cell Membrane by Auger Electrons Is Cytotoxic Through Oxidative Stress-Mediated Nontargeted Effects. Antioxidants & redox signaling. 25(8):467–484. [PubMed: 27224059]

Panosa C, Fonge H, Ferrer-Batalle M, Menendez JA, Massaguer A, De Llorens R, Reilly RM. 2015. A comparison of non-biologically active truncated EGF (EGFt) and full-length hEGF for delivery of Auger electron-emitting 111In to EGFR-positive breast cancer cells and tumor xenografts in athymic mice. Nucl Med Biol. 42(12):931–938. [PubMed: 26385534]

Panyutin IG, Neumann RD. 1994. Sequence-specific DNA double-strand breaks induced by triplex forming ^{125}I labeled oligonucleotides. Nucleic Acids Res. 22(23):4979–4982. [PubMed: 7800489]

Panyutin IG, Winters TA, Feinendegen LE, Neumann RD. 2000. Development of DNA-based radiopharmaceuticals carrying Auger-electron emitters for anti-gene radiotherapy. Q J Nucl Med. 44(3):256–267. eng. [PubMed: 11105589]

Paro AD, Shanmugam I, van de Ven AL. 2017. Nanoparticle-Mediated X-Ray Radiation Enhancement for Cancer Therapy. Methods in molecular biology. 1530:391–401. [PubMed: 28150217]

Pasternack JB, Domogauer JD, Khullar A, Akudugu JM, Howell RW. 2014. The advantage of antibody cocktails for targeted alpha therapy depends on specific activity. J Nucl Med. 55(12):2012–2019. [PubMed: 25349219]

Peng YG, Wu Y, Zhu LF, Zhang SB, Wang JG, Liebermann HP, Buenker RJ. 2016. Complex multireference configuration interaction calculations for the K-vacancy Auger states of N(q+) (q = 2–5) ions. The Journal of chemical physics. 144(5):054306. [PubMed: 26851920]

Pereira E, do Quental L, Palma E, Oliveira MC, Mendes F, Raposinho P, Correia I, Lavrado J, Di Maria S, Belchior A et al. 2017. Evaluation of Acridine Orange Derivatives as DNA-Targeted Radiopharmaceuticals for Auger Therapy: Influence of the Radionuclide and Distance to DNA. Scientific reports. 7:42544. [PubMed: 28211920]

Pernpointner M, Knecht S. 2005. The influence of relativistic effects on the ionization spectra of the alkali iodides. Chemical Physics Letters. 410:423–429.

Pernpointner M, Knecht S, Cederbaum LS. 2006. Ionization spectra and electronic decay in small iodide clusters: fully relativistic results. The Journal of chemical physics. 125(3):34309. eng. [PubMed: 16863352]

Peters T, Grunewald C, Blaickner M, Ziegner M, Schutz C, Iffland D, Hampel G, Nawroth T, Langguth P. 2015. Cellular uptake and in vitro antitumor efficacy of composite liposomes for neutron capture therapy. Radiat Oncol. 10:52. [PubMed: 25889824]

Piron B, Paillas S, Boudousq V, Pelegrin A, Bascoul-Mollevi C, Chouin N, Navarro-Teulon I, Pouget JP. 2014. DNA damage-centered signaling pathways are effectively activated during low dose-rate Auger radioimmunotherapy. Nucl Med Biol. 41 Suppl:e75–83. [PubMed: 24613681]

Piroozfar B, Raisali G, Alirezapour B, Mirzaii M. 2018. The effect of ^{111}In radionuclide distance and auger electron energy on direct induction of DNA double-strand breaks: a Monte Carlo study using Geant4 toolkit. International journal of radiation biology. 94(4):385–393. [PubMed: 29432072]

Pomplun E 2000. Auger electron spectra--the basic data for understanding the Auger effect. Acta oncologica. 39(6):673–679. [PubMed: 11130003]

Pomplun E 2016. Monte Carlo simulation of Auger electron cascades versus experimental data. Biomed Phys Eng Express. 2(1):015014.

Pomplun E, Booz J, Charlton DE. 1987. A Monte Carlo simulation of Auger cascades. Radiat Res. 111:533–552. [PubMed: 3659286]

Pomplun E, Sutmann G. 2004. Is coulomb explosion a damaging mechanism for 125IUdR? International journal of radiation biology. 80(11–12):855–860. eng. [PubMed: 15764393]

Pouget JP, Georgakilas AG, Ravanat JL. 2018. Targeted and Off-Target (Bystander and Abscopal) Effects of Radiation Therapy: Redox Mechanisms and Risk/Benefit Analysis. Antioxidants & redox signaling. 29(15):1447–1487. [PubMed: 29350049]

Pouget JP, Santoro L, Raymond L, Chouin N, Bardies M, Bascoul-Mollevi C, Huguet H, Azria D, Kotzki PO, Pelegrin M et al. 2008. Cell membrane is a more sensitive target than cytoplasm to dense ionization produced by auger electrons. Radiat Res. 170(2):192–200. [PubMed: 18666820]

Prise KM, O'Sullivan JM. 2009. Radiation-induced bystander signalling in cancer therapy. Nature reviews Cancer. 9(5):351–360. [PubMed: 19377507]

Pronschinske A, Pedevilla P, Coughlin B, Murphy CJ, Lucci FR, Payne MA, Gellman AJ, Michaelides A, Sykes EC. 2016. Atomic-Scale Picture of the Composition, Decay, and Oxidation of Two-Dimensional Radioactive Films. ACS nano. 10(2):2152–2158. [PubMed: 26735687]

Protti N, Geninatti-Crich S, Alberti D, Lanzardo S, Deagostino A, Toppino A, Aime S, Ballarini F, Bortolussi S, Bruschi P et al. 2015. Evaluation of the dose enhancement of combined ^{10}B + ^{157}Gd neutron capture therapy (NCT). Radiation protection dosimetry. 166(1–4):369–373. [PubMed: 26246584]

Qaim SM, Spahn I. 2018. Development of novel radionuclides for medical applications. Journal of labelled compounds & radiopharmaceuticals. 61(3):126–140. [PubMed: 29110328]

Raghavan R, Howell RW, Zalutsky MR. 2017. A model for optimizing delivery of targeted radionuclide therapies into resection cavity margins for the treatment of primary brain cancers. Biomedical physics & engineering express. 3(3).

Rakowski JT, Laha SS, Snyder MG, Buczek MG, Tucker MA, Liu F, Mao G, Hillman Y, Lawes G. 2015. Measurement of gold nanofilm dose enhancement using unlaminated radiochromic film. Med Phys. 42(10):5937–5944. [PubMed: 26429268]

Rao DV, Narra VR, Govelitz GF, Lanka VK, Howell RW, Sastry KSR. 1990. In vivo effects of 5.3 MeV alpha particles from Po-210 in mouse testes: Comparison with internal Auger emitters. Radiat Prot Dosim. 31:329–332.

Reijonen V, Kanninen LK, Hippelainen E, Lou YR, Salli E, Sofiev A, Malinen M, Paasonen T, Yliperttula M, Kuronen A et al. 2017. Multicellular dosimetric chain for molecular radiotherapy exemplified with dose simulations on 3D cell spheroids. Physica medica : PM : an international journal devoted to the applications of physics to medicine and biology : official journal of the Italian Association of Biomedical Physics. 40:72–78.

Reissig F, Mamat C, Steinbach J, Pietzsch HJ, Freudenberg R, Navarro-Retamal C, Caballero J, Kotzerke J, Wunderlich G. 2016. Direct and Auger Electron-Induced, Single- and Double-Strand Breaks on Plasmid DNA Caused by 99mTc-Labeled Pyrene Derivatives and the Effect of Bonding Distance. PLoS One. 11(9):e0161973. [PubMed: 27583677]

Retif P, Bastogne T, Barberi-Heyob M. 2016. Robustness Analysis of a Geant4-GATE Simulator for Nanoradiosensitizers Characterization. IEEE transactions on nanobioscience. 15(3):209–217. [PubMed: 26887000]

Rezaee M, Hill RP, Jaffray DA. 2017. The Exploitation of Low-Energy Electrons in Cancer Treatment. Radiat Res. 188(2):123–143. [PubMed: 28557630]

Righi S, Ugolini M, Bottoni G, Puntoni M, Iacozzi M, Paparo F, Cabria M, Ceriani L, Gambaro M, Giovanella L et al. 2018. Biokinetic and dosimetric aspects of (64)CuCl2 in human prostate cancer: possible theranostic implications. EJNMMI research. 8(1):18. [PubMed: 29492782]

Roos AH, Eland JH, Andersson J, Zagorodskikh S, Singh R, Squibb RJ, Feifel R. 2016. Relative extent of double and single Auger decay in molecules containing C, N and O atoms. Physical chemistry chemical physics : PCCP. 18(36):25705–25710. [PubMed: 27711372]

Roos AH, Eland JHD, Andersson J, Squibb RJ, Koulentianos D, Talaee O, Feifel R. 2018. Abundance of molecular triple ionization by double Auger decay. Scientific reports. 8(1):16405. [PubMed: 30401877]

Rosenkranz AA, Slastnikova TA, Karmakova TA, Vorontsova MS, Morozova NB, Petriev VM, Abrosimov AS, Khramtsov YV, Lupanova TN, Ulasov AV et al. 2018. Antitumor Activity of Auger Electron Emitter [111]In Delivered by Modular Nanotransporter for Treatment of Bladder Cancer With EGFR Overexpression. Frontiers in pharmacology. 9:1331. [PubMed: 30510514]

Roteta M, Fernandez-Martinez R, Mejuto M, Rucandio I. 2016. Preparation of graphene thin films for radioactive samples. Applied radiation and isotopes : including data, instrumentation and methods for use in agriculture, industry and medicine. 109:217–221. [PubMed: 26651168]

Royle G, Falzone N, Chakalova R, Vallis K, Myhra S. 2016. Internalization of Auger electron-emitting isotopes into cancer cells: a method for spatial distribution determination of equivalent source terms. International journal of radiation biology. 92(11):633–640. [PubMed: 27603222]

Royle G, Myhra S, Chakalova R, Vallis KA, Falzone N. 2015. Spatial distribution of Auger electrons emitted from internalised radionuclides in cancer cells: the photoresist autoradiography (PAR) method. Radiation protection dosimetry. 166(1–4):228–232. [PubMed: 25889606]

Runge R, Oehme L, Kotzerke J, Freudenberg R. 2016. The effect of dimethyl sulfoxide on the induction of DNA strand breaks in plasmid DNA and colony formation of PC Cl3 mammalian cells by alpha-, beta-, and Auger electron emitters ^{223}Ra, ^{188}Re, and ^{99m}Tc. EJNMMI research. 6(1):48. [PubMed: 27259575]

Sahu SK, Kassis AI, Makrigiorgos GM, Baranowksa-Kortylewicz J, Adelstein SJ. 1995. The effects of indium-111 decay on pBR322 DNA. Radiat Res. 147(4):401–408.

Sakata D, Kyriakou I, Tran HN, Bordage MC, Rosenfeld A, Ivanchenko V, Incerti S, Emfietzoglou D, Guatelli S. 2019. Electron track structure simulations in a gold nanoparticle using Geant4-DNA. Physica medica : PM : an international journal devoted to the applications of physics to medicine and biology : official journal of the Italian Association of Biomedical Physics. 63:98–104.

Saleh T, Bloukh S, Carpenter VJ, Alwohoush E, Bakeer J, Darwish S, Azab B, Gewirtz DA. 2020. Therapy-Induced Senescence: An "Old" Friend Becomes the Enemy. Cancers. 12(4).

Salim R, Taherparvar P. 2019. Monte Carlo single-cell dosimetry using Geant4-DNA: the effects of cell nucleus displacement and rotation on cellular S values. Radiat Environ Biophys.

Sann H, Havermeier T, Muller C, Kim HK, Trinter F, Waitz M, Voigtsberger J, Sturm F, Bauer T, Wallauer R et al. 2016. Imaging the Temporal Evolution of Molecular Orbitals during Ultrafast Dissociation. Physical review letters. 117(24):243002. [PubMed: 28009186]

Santoro L, Boutaleb S, Garambois V, Bascoul-Mollevi C, Boudousq V, Kotzki PO, Pelegrin M, Navarro-Teulon I, Pelegrin A, Pouget JP. 2009. Noninternalizing monoclonal antibodies are suitable candidates for 125I radioimmunotherapy of small-volume peritoneal carcinomatosis. J Nucl Med. 50(12):2033–2041. [PubMed: 19910417]

Santos ACF, Vasconcelos DN, MacDonald MA, Sant'Anna MM, Tenorio BNC, Rocha AB, Morcelle V, Appathurai N, Zuin L. 2018. Atomic versus molecular Auger decay in CH2Cl2 and CD2Cl2 molecules. The Journal of chemical physics. 149(5):054303. [PubMed: 30089389]

Sastry KS. 1992. Biological effects of the Auger emitter iodine-^{125}: a review. Report No. 1 of AAPM Nuclear Medicine Task Group No. 6. Med Phys. 19(6):1361–1370. [PubMed: 1461198]

Sastry KSR. 1992. Biological effects of the Auger emitter ^{125}I: A review. Report No. 1 of AAPM Nuclear Medicine Task Group No. 6. Med Phys. 19(6):1361–1370. [PubMed: 1461198]

Sastry KSR, Rao DV. 1984. Dosimetry of low energy electrons. In: Rao DV, Chandra R, Graham M, editors. Physics of Nuclear Medicine: Recent Advances. New York: American Institute of Physics; p. 169–208.

Schipper ML, Riese CG, Seitz S, Weber A, Behe M, Schurrat T, Schramm N, Keil B, Alfke H, Behr TM. 2007. Efficacy of (^{99m})Tc pertechnetate and (^{131})I radioisotope therapy in sodium/iodide symporter (NIS)-expressing neuroendocrine tumors in vivo. European journal of nuclear medicine and molecular imaging. 34(5):638–650. eng. [PubMed: 17160413]

Schmitz S, Oskamp D, Pomplun E, Kriehuber R. 2015. Chromosome aberrations induced by the Auger electron emitter ^{125}I. Mutation research Genetic toxicology and environmental mutagenesis. 793:64–70. [PubMed: 26520374]

Schmitz S, Oskamp D, Pomplun E, Kriehuber R. 2016. Corrigendum to "Chromosome aberrations induced by the Auger electron emitter [125]I" [Mut. Res.-Genet. Toxicol. Environ. Mutagen. 793 (2015) 64–70]. Mutation research Genetic toxicology and environmental mutagenesis. 800–801:46.

Sefl M, Incerti S, Papamichael G, Emfietzoglou D. 2015. Calculation of cellular S-values using Geant4-DNA: The effect of cell geometry. Applied radiation and isotopes : including data, instrumentation and methods for use in agriculture, industry and medicine. 104:113–123. [PubMed: 26159660]

Seifi Moradi M, Shirani Bidabadi B. 2018. Micro-dosimetry calculation of Auger-electron-emitting radionuclides mostly used in nuclear medicine using GEANT4-DNA. Applied radiation and isotopes : including data, instrumentation and methods for use in agriculture, industry and medicine. 141:73–79. [PubMed: 30179772]

Shinohara A, Hanaoka H, Sakashita T, Sato T, Yamaguchi A, Ishioka NS, Tsushima Y. 2018. Rational evaluation of the therapeutic effect and dosimetry of auger electrons for radionuclide therapy in a cell culture model. Annals of nuclear medicine. 32(2):114–122. [PubMed: 29238922]

Siragusa M, Baiocco G, Fredericia PM, Friedland W, Groesser T, Ottolenghi A, Jensen M. 2017. The COOLER Code: A Novel Analytical Approach to Calculate Subcellular Energy Deposition by Internal Electron Emitters. Radiation research. 188(2):204–220. [PubMed: 28621586]

Sisourat N, Engin S, Gorfinkiel JD, Kazandjian S, Kolorenc P, Miteva T. 2017. On the computations of interatomic Coulombic decay widths with R-matrix method. The Journal of chemical physics. 146(24):244109. [PubMed: 28668042]

Sisourat N, Kazandjian S, Miteva T. 2017. Probing Conformers of Benzene Dimer with Intermolecular Coulombic Decay Spectroscopy. The journal of physical chemistry A. 121(1):45–50. [PubMed: 27976576]

Slastnikova TA, Rosenkranz AA, Khramtsov YV, Karyagina TS, Ovechko SA, Sobolev AS. 2017. Development and evaluation of a new modular nanotransporter for drug delivery into nuclei of pathological cells expressing folate receptors. Drug design, development and therapy. 11:1315–1334. [PubMed: 28490863]

Slastnikova TA, Rosenkranz AA, Morozova NB, Vorontsova MS, Petriev VM, Lupanova TN, Ulasov AV, Zalutsky MR, Yakubovskaya RI, Sobolev AS. 2017. Preparation, cytotoxicity, and in vivo antitumor efficacy of ^{111}In-labeled modular nanotransporters. International journal of nanomedicine. 12:395–410. [PubMed: 28138237]

Slastnikova TA, Rosenkranz AA, Zalutsky MR, Sobolev AS. 2015. Modular nanotransporters for targeted intracellular delivery of drugs: folate receptors as potential targets. Current pharmaceutical design. 21(9):1227–1238. [PubMed: 25312738]

Sobolev AS. 2018. Modular Nanotransporters for Nuclear-Targeted Delivery of Auger Electron Emitters. Frontiers in pharmacology. 9:952. [PubMed: 30210340]

Sokolov MV, Smirnova NA, Camerini-Otero RD, Neumann RD, Panyutin IG. 2006. Microarray analysis of differentially expressed genes after exposure of normal human fibroblasts to ionizing radiation from an external source and from DNA-incorporated iodine-125 radionuclide. Gene. 382:47–56. [PubMed: 16876969]

Song L, Falzone N, Vallis KA. 2016. EGF-coated gold nanoparticles provide an efficient nano-scale delivery system for the molecular radiotherapy of EGFR-positive cancer. International journal of radiation biology. 92(11):716–723. [PubMed: 26999580]

Spencer JA, Barclay M, Gallagher MJ, Winkler R, Unlu I, Wu YC, Plank H, McElwee-White L, Fairbrother DH. 2017. Comparing postdeposition reactions of electrons and radicals with Pt nanostructures created by focused electron beam induced deposition. Beilstein journal of nanotechnology. 8:2410–2424. [PubMed: 29234576]

Spencer JA, Wu YC, McElwee-White L, Fairbrother DH. 2016. Electron Induced Surface Reactions of cis-PtCO$_2$Cl$_2$: A Route to Focused Electron Beam Induced Deposition of Pure Pt Nanostructures. Journal of the American Chemical Society. 138(29):9172–9182. [PubMed: 27346707]

Sreedharan S, Gill MR, Garcia E, Saeed HK, Robinson D, Byrne A, Cadby A, Keyes TE, Smythe C, Pellett P et al. 2017. Multimodal Super-resolution Optical Microscopy Using a Transition-Metal-Based Probe Provides Unprecedented Capabilities for Imaging Both Nuclear Chromatin

and Mitochondria. Journal of the American Chemical Society. 139(44):15907–15913. [PubMed: 28976195]

Sung W, Jung S, Ye SJ. 2016. Evaluation of the microscopic dose enhancement for nanoparticle-enhanced Auger therapy. Phys Med Biol. 61(21):7522–7535. [PubMed: 27716643]

Taborda A, Benabdallah N, Desbree A. 2016. Dosimetry at the sub-cellular scale of Auger-electron emitter 99mTc in a mouse single thyroid follicle. Applied radiation and isotopes : including data, instrumentation and methods for use in agriculture, industry and medicine. 108:58–63. [PubMed: 26704702]

Taha E, Djouider F, Banoqitah E. 2018. Monte Carlo simulations for dose enhancement in cancer treatment using bismuth oxide nanoparticles implanted in brain soft tissue. Australasian physical & engineering sciences in medicine. 41(2):363–370. [PubMed: 29582243]

Takanashi T, Nakamura K, Kukk E, Motomura K, Fukuzawa H, Nagaya K, Wada SI, Kumagai Y, Iablonskyi D, Ito Y et al. 2017. Ultrafast Coulomb explosion of a diiodomethane molecule induced by an X-ray free-electron laser pulse. Physical chemistry chemical physics : PCCP. 19(30):19707–19721. [PubMed: 28530728]

Tang CY, Haasch RT, Dillon SJ. 2016. In situ X-ray photoelectron and Auger electron spectroscopic characterization of reaction mechanisms during Li-ion cycling. Chem Commun (Camb). 52(90):13257–13260. [PubMed: 27775104]

Taupin F, Flaender M, Delorme R, Brochard T, Mayol JF, Arnaud J, Perriat P, Sancey L, Lux F, Barth RF et al. 2015. Gadolinium nanoparticles and contrast agent as radiation sensitizers. Phys Med Biol. 60(11):4449–4464. [PubMed: 25988839]

Terrissol M 2016. Pierre Auger and Monte Carlo. Int J Radiat Biol. 92(11):616. [PubMed: 27834586]

Thisgaard H, Halle B, Aaberg-Jessen C, Olsen BB, Therkelsen AS, Dam JH, Langkjaer N, Munthe S, Nagren K, Hoilund-Carlsen PF et al. 2016. Highly Effective Auger-Electron Therapy in an Orthotopic Glioblastoma Xenograft Model using Convection-Enhanced Delivery. Theranostics. 6(12):2278–2291. [PubMed: 27924163]

Tomita M, Maeda M, Usami N, Yokoya A, Watanabe R, Kobayashi K. 2016. Enhancement of DNA double-strand break induction and cell killing by K-shell absorption of phosphorus in human cell lines. Int J Radiat Biol. 92(11):724–732. [PubMed: 27185241]

Travnikova O, Sisourat N, Marchenko T, Goldsztejn G, Guillemin R, Journel L, Ceolin D, Ismail I, Lago AF, Puttner R et al. 2017. Subfemtosecond Control of Molecular Fragmentation by Hard X-Ray Photons. Physical review letters. 118(21):213001. [PubMed: 28598654]

Tsai WK, Wu AM. 2018. Aligning physics and physiology: Engineering antibodies for radionuclide delivery. Journal of labelled compounds & radiopharmaceuticals. 61(9):693–714. [PubMed: 29537104]

Unverricht-Yeboah M, Giesen U, Kriehuber R. 2018. Comparative gene expression analysis after exposure to 123I-iododeoxyuridine, gamma- and alpha-radiation-potential biomarkers for the discrimination of radiation qualities. Journal of radiation research (Tokyo). 59(4):411–429.

Uusijärvi H, Bernhardt P, Ericsson T, Forssell-Aronsson E. 2006. Dosimetric characterization of radionuclides for systemic tumor therapy: influence of particle range, photon emission, and subcellular distribution. Medical physics. 33(9):3260–3269. eng. [PubMed: 17022220]

Valdovinos HF, Hernandez R, Graves S, Ellison PA, Barnhart TE, Theuer CP, Engle JW, Cai W, Nickles RJ. 2017. Cyclotron production and radiochemical separation of ^{55}Co and ^{58m}Co from ^{54}Fe, ^{58}Ni and ^{57}Fe targets. Applied radiation and isotopes : including data, instrumentation and methods for use in agriculture, industry and medicine. 130:90–101. [PubMed: 28946101]

Vaxenburg R, Rodina A, Shabaev A, Lifshitz E, Efros AL. 2015. Nonradiative Auger recombination in semiconductor nanocrystals. Nano letters. 15(3):2092–2098. [PubMed: 25693512]

Vaziri B, Wu H, Dhawan AP, Du P, Howell RW. 2014. MIRD Pamphlet No. 25: MIRDcell V2.0 Software Tool for Dosimetric Analysis of Biologic Response of Multicellular Populations. J Nucl Med. 55(9):1557–1564. [PubMed: 25012457]

Villagomez-Bernabe B, Currell FJ. 2019. Physical Radiation Enhancement Effects Around Clinically Relevant Clusters of Nanoagents in Biological Systems. Scientific reports. 9(1):8156. [PubMed: 31148555]

Violet JA, Farrugia G, Skene C, White J, Lobachevsky P, Martin R. 2016. Triple targeting of Auger emitters using octreotate conjugated to a DNA-binding ligand and a nuclear localizing signal. Int J Radiat Biol. 92(11):707–715. [PubMed: 27010622]

Vultos F, Fernandes C, Mendes F, Marques F, Correia JDG, Santos I, Gano L. 2017. A Multifunctional Radiotheranostic Agent for Dual Targeting of Breast Cancer Cells. ChemMedChem. 12(14):1103–1107. [PubMed: 28628723]

Walicka MA, Adelstein SJ, Kassis AI. 1998a. Indirect mechansims contribute to biological effects produced by decay of DNA-incorporated iodine-125 in mammalian cells *in vitro*: Clonogenic survival. Radiat Res. 149:142–146. [PubMed: 9457893]

Walicka MA, Adelstein SJ, Kassis AI. 1998b. Indirect mechansims contribute to biological effects produced by decay of DNA-incorporated iodine-125 in mammalian cells *in vitro*: Double-strand breaks. Radiat Res. 149:134–141. [PubMed: 9457892]

Walicka MA, Ding Y, Adelstein SJ, Kassis AI. 2000. Toxicity of DNA-incorporated iodine-125: Quantifying the direct and indirect effects. Radiat Res. 154:326–330. [PubMed: 10956440]

Walther M, Preusche S, Bartel S, Wunderlich G, Freudenberg R, Steinbach J, Pietzsch HJ. 2015. Theranostic mercury: ^{197m}Hg with high specific activity for imaging and therapy. Applied radiation and isotopes : including data, instrumentation and methods for use in agriculture, industry and medicine. 97:177–181. [PubMed: 25588997]

Wang C, Sun A, Qiao Y, Zhang P, Ma L, Su M. 2015. Cationic surface modification of gold nanoparticles for enhanced cellular uptake and X-ray radiation therapy. Journal of materials chemistry B. 3(37):7372–7376. [PubMed: 26512323]

Wang H, Zhang C, Rana F. 2015. Ultrafast dynamics of defect-assisted electron-hole recombination in monolayer MoS2. Nano letters. 15(1):339–345. [PubMed: 25546602]

Watanabe R, Hattori Y, Kai T. 2016. Evaluation of DNA damage induced by Auger electrons from ^{137}Cs. International journal of radiation biology. 92(11):660–664. [PubMed: 27010691]

Widel M 2017. Radionuclides in radiation-induced bystander effect; may it share in radionuclide therapy? Neoplasma. 64(5):641–654. [PubMed: 28592116]

Won S, Huh YH, Cho LR, Lee HS, Byon ES, Park CJ. 2017. Cellular Response of Human Bone Marrow Derived Mesenchymal Stem Cells to Titanium Surfaces Implanted with Calcium and Magnesium Ions. Tissue engineering and regenerative medicine. 14(2):123–131. [PubMed: 30603469]

Wragg A, Gill MR, McKenzie L, Glover C, Mowll R, Weinstein JA, Su X, Smythe C, Thomas JA. 2015. Serum Albumin Binding Inhibits Nuclear Uptake of Luminescent Metal-Complex-Based DNA Imaging Probes. Chemistry. 21(33):11865–11871. [PubMed: 26133680]

Wright HA, Hamm RN, Turner JE, Howell RW, Rao DV, Sastry KSR. 1990. Calculations of physical and chemical reactions with DNA in aqueous solution from Auger cascades. Radiat Prot Dosim. 31:59–62.

Xie WZ, Friedland W, Li WB, Li CY, Oeh U, Qiu R, Li JL, Hoeschen C. 2015. Simulation on the molecular radiosensitization effect of gold nanoparticles in cells irradiated by x-rays. Phys Med Biol. 60(16):6195–6212. [PubMed: 26226203]

Xu X, Chong Y, Liu X, Fu H, Yu C, Huang J, Zhang Z. 2019. Multifunctional nanotheranostic gold nanocages for photoacoustic imaging guided radio/photodynamic/photothermal synergistic therapy. Acta biomaterialia. 84:328–338. [PubMed: 30500447]

Xue LY, Butler NJ, Makrigiorgos GM, Adelstein SJ, Kassis AI. 2002. Bystander effect produced by radiolabeled tumor cells in vivo. Proc Natl Acad Sci U S A. 99(21):13765–13770. [PubMed: 12368480]

Yasui LS. 2012. Molecular and cellular effects of Auger emitters: 2008–2011. Int J Radiat Biol. 88(12):864–870. [PubMed: 22694308]

Yasui LS, Duran M, Andorf C, Kroc T, Owens K, Allen-Durdan K, Schuck A, Grayburn S, Becker R. 2016. Autophagic flux in glioblastoma cells. Int J Radiat Biol. 92(11):665–678. [PubMed: 26967573]

Yokoya A 2016. The 8th Auger Symposium: Preface. Int J Radiat Biol. 92(11):614–615. [PubMed: 27094732]

Yokoya A, Ito T. 2017. Photon-induced Auger effect in biological systems: a review. Int J Radiat Biol. 93(8):743–756. [PubMed: 28397587]

You D, Fukuzawa H, Sakakibara Y, Takanashi T, Ito Y, Maliyar GG, Motomura K, Nagaya K, Nishiyama T, Asa K et al. 2017. Charge transfer to ground-state ions produces free electrons. Nature communications. 8:14277.

Zhang P, Qiao Y, Xia J, Guan J, Ma L, Su M. 2015. Enhanced radiation therapy with multilayer microdisks containing radiosensitizing gold nanoparticles. ACS applied materials & interfaces. 7(8):4518–4524. [PubMed: 25679345]

Zhu C, Sempkowski M, Holleran T, Linz T, Bertalan T, Josefsson A, Bruchertseifer F, Morgenstern A, Sofou S. 2017. Alpha-particle radiotherapy: For large solid tumors diffusion trumps targeting. Biomaterials. 130:67–75. [PubMed: 28365545]

Zhu Y, Zhang M, Luo L, Gill MR, De Pace C, Battaglia G, Zhang Q, Zhou H, Wu J, Tian Y et al. 2019. NF-kappaB hijacking theranostic Pt(ll) complex in cancer therapy. Theranostics. 9(8):2158–2166. [PubMed: 31149035]
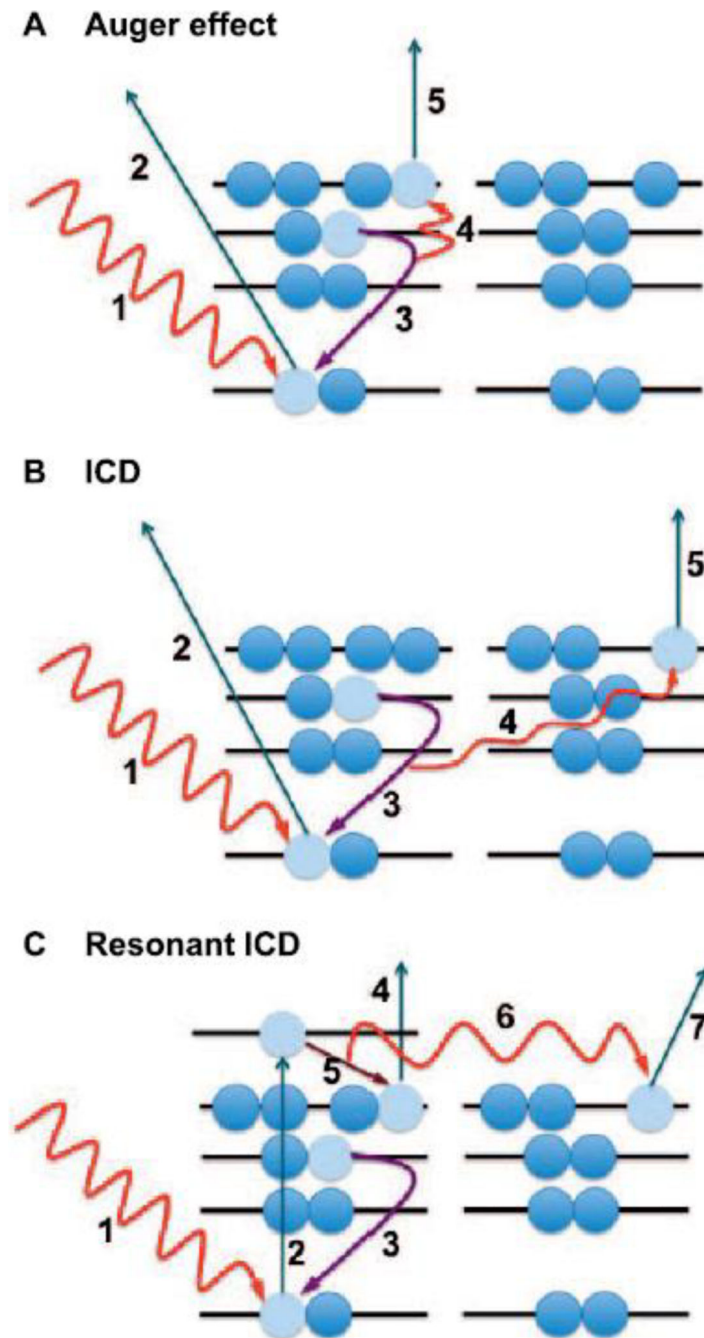
Figure 1.

Atomic and molecular processes that follow the creation of an initial vacancy in an inner atomic shell and result in the emission of low energy electrons. The initial vacancy can be created by external radiation (e.g. photoelectric effect), or nuclear decay processes including electron capture and internal conversion. Creation of the vacancy is followed by either an Auger transition (top), intermolecular Coulombic decay (ICD) (middle), or resonant ICD (bottom). For Auger transition, numbered arrows represent the following: (1) process responsible for removing inner shell electron, (2) removal of inner shell electron, (3)

electron from higher orbital that fills initial inner shell vacancy, (4) transfer of excess energy to an electron in the same atom, (5) ejected Auger electron. For ICD: (1) process responsible for removing inner shell electron, (2) removal of inner shell electron, (3) electron from higher orbital that fills initial inner shell vacancy, (4) transfer of energy to an electron in neighboring atom, (5) electron ejected from neighboring atom. For resonant ICD: (1) process responsible for *exciting* inner shell electron, (2) inner shell electron excited to higher shell, (3) electron from higher orbital that fills inner shell vacancy and (4) electron is ejected, (5) excited electron fills vacancy and transfers energy (6) to electron in neighboring atom (7) which is ejected. These processes compete with X-ray emission as the excited molecular states rapidly return to the ground state. This leads to a cascade of electron transitions that release a shower of low energy electrons. Adopted from Rezaee et al. (Rezaee et al. 2017).
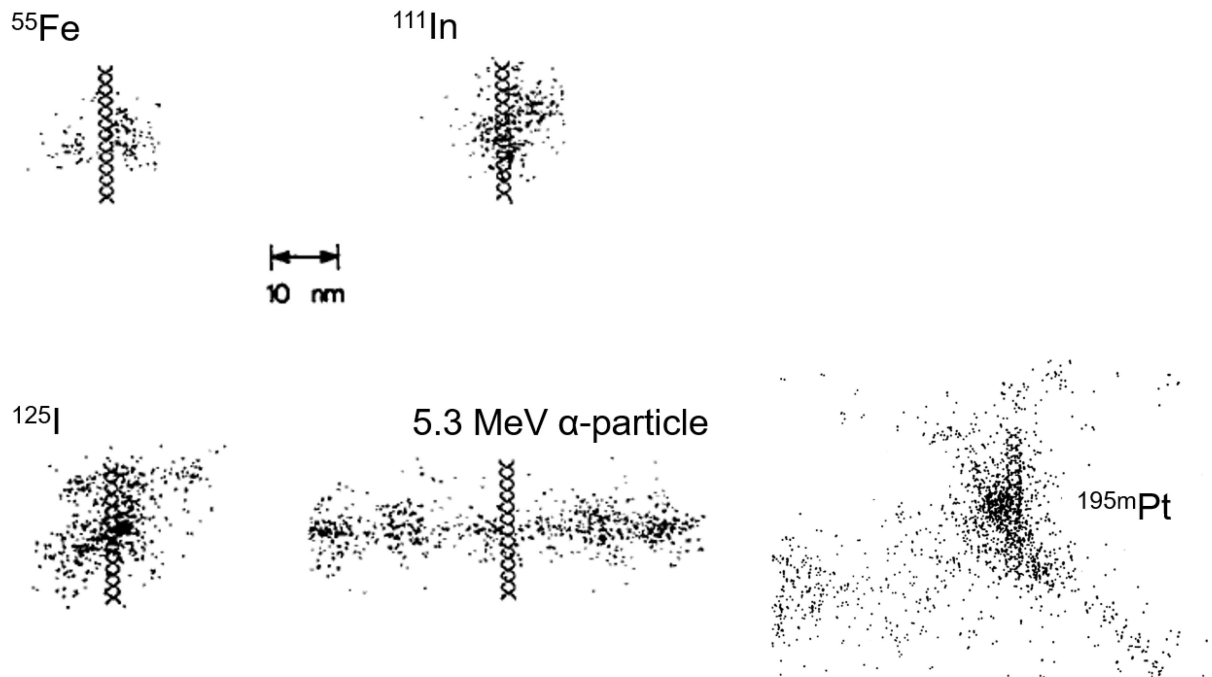
Figure 2.
Initial positions of reactive chemical species produced in water by Auger cascades compared to those along the track of a 5.3-MeV α-particle. The two helical strands of simulated DNA are depicted (reproduced from (Wright et al. 1990; Howell et al. 1994). An average of 5, 15, 25, and 33 Auger electrons per decay are emitted by ^{55}Fe, ^{111}In, ^{125}I, and ^{195m}Pt respectively (Howell 1992).
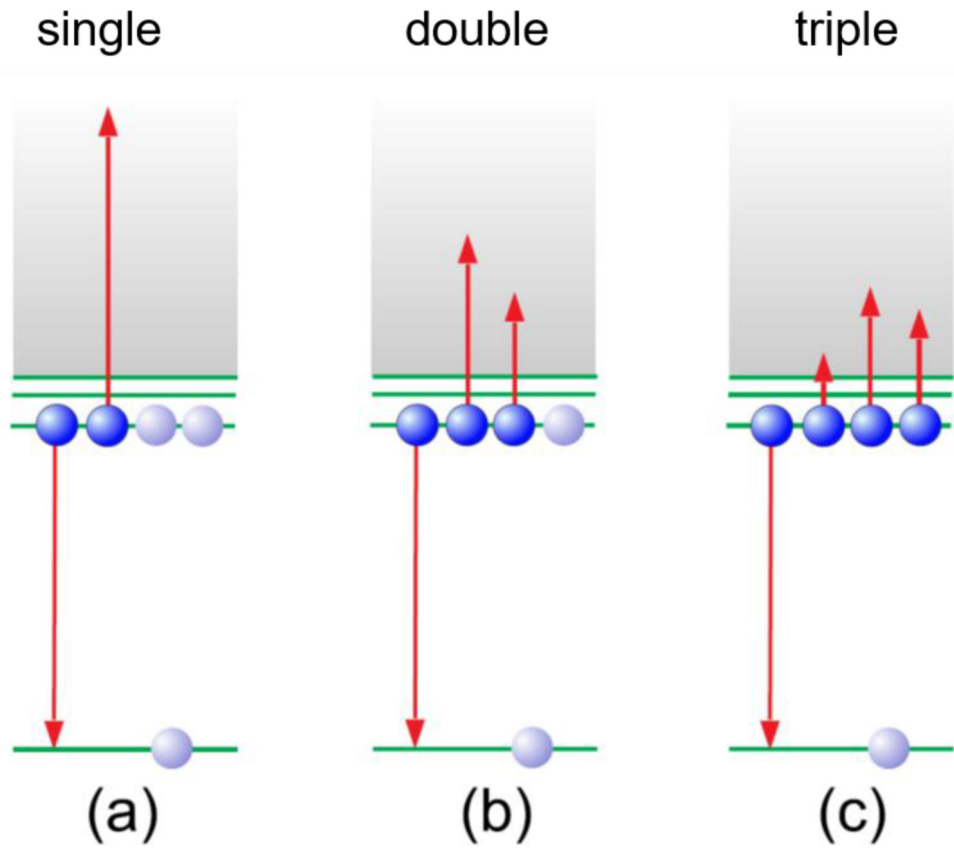
Figure 3.
Depiction of electronic subshells for single, double, and triple Auger decay. An inner atomic shell vacancy is filled by an electron in a higher shell with concomitant emission of: (a) single Auger electron, (b) two Auger electrons, or (c) three Auger electrons. Adapted from Müller et al. (Muller A et al. 2015).
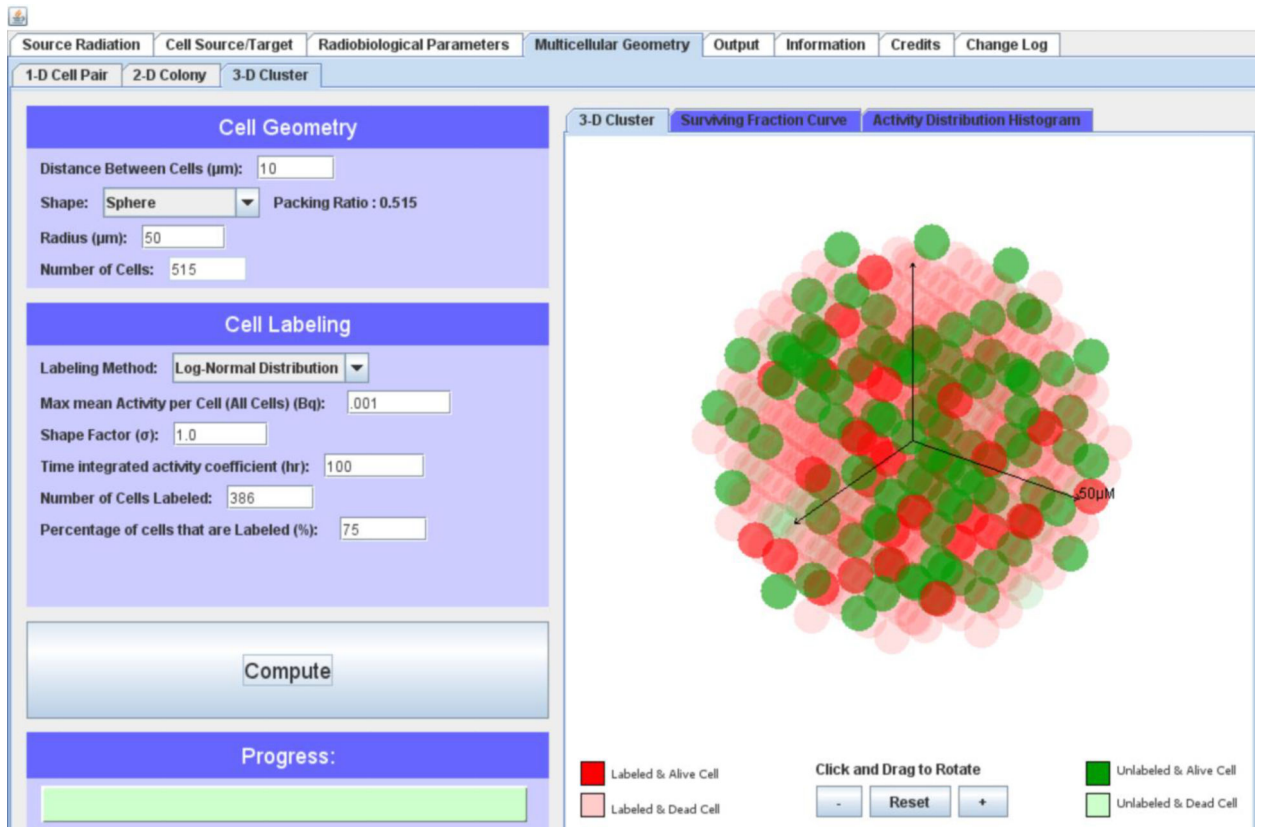
Figure 4.
Screenshot of MIRDcell V2.17 software tool for multicellular dosimetry and modeling of radiobiological response (Vaziri et al. 2014). Spherical cluster (radius 50 μm) containing 515 cells with 75% labeled with [125]I (red) and 25% unlabeled (green).
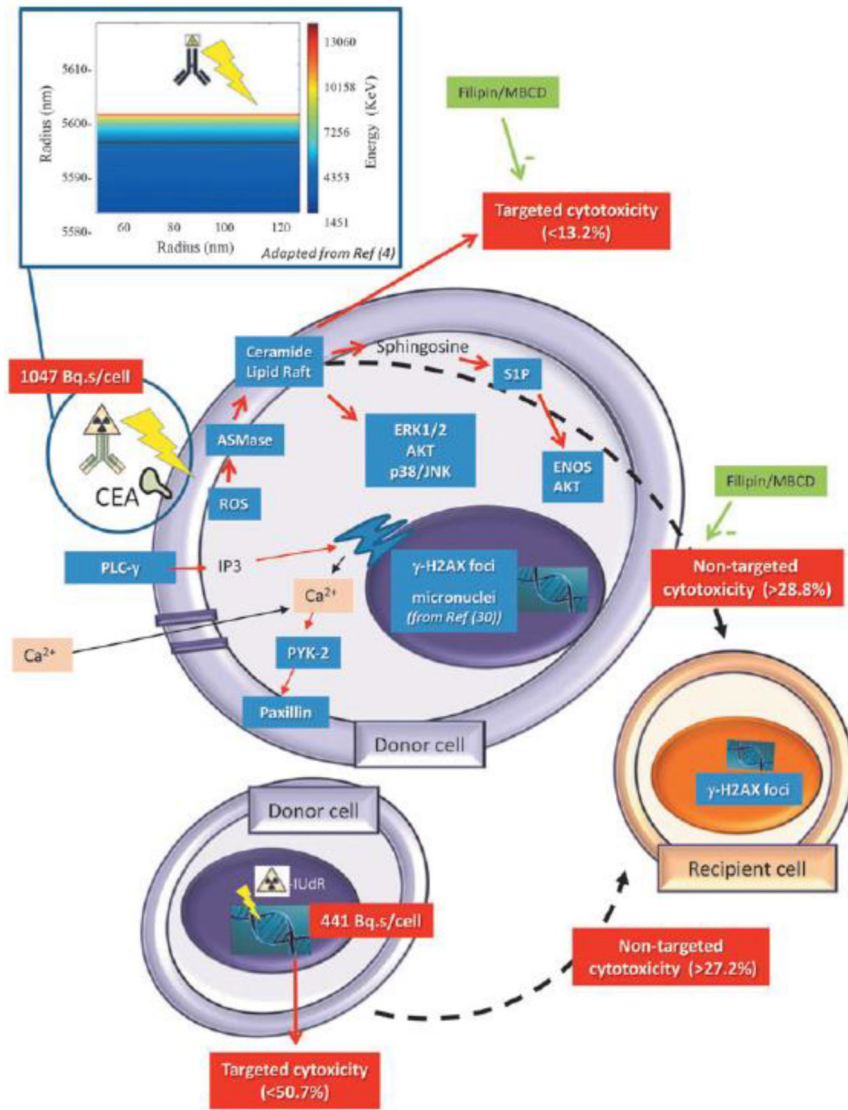
Figure 5.
Schematic of the mechanisms involved in radioimmunotherapy using ^{125}I labeled monoclonal antibodies (^{125}I-mAbs). These radiopharmaceuticals target the cell membrane and deliver high and localized energy at the cell surface. Lipid raft-dependent radiation-induced bystander effects, including cytotoxicity and γH2AX formation, are observed in neighboring cells. Adopted from (Paillas et al. 2016).
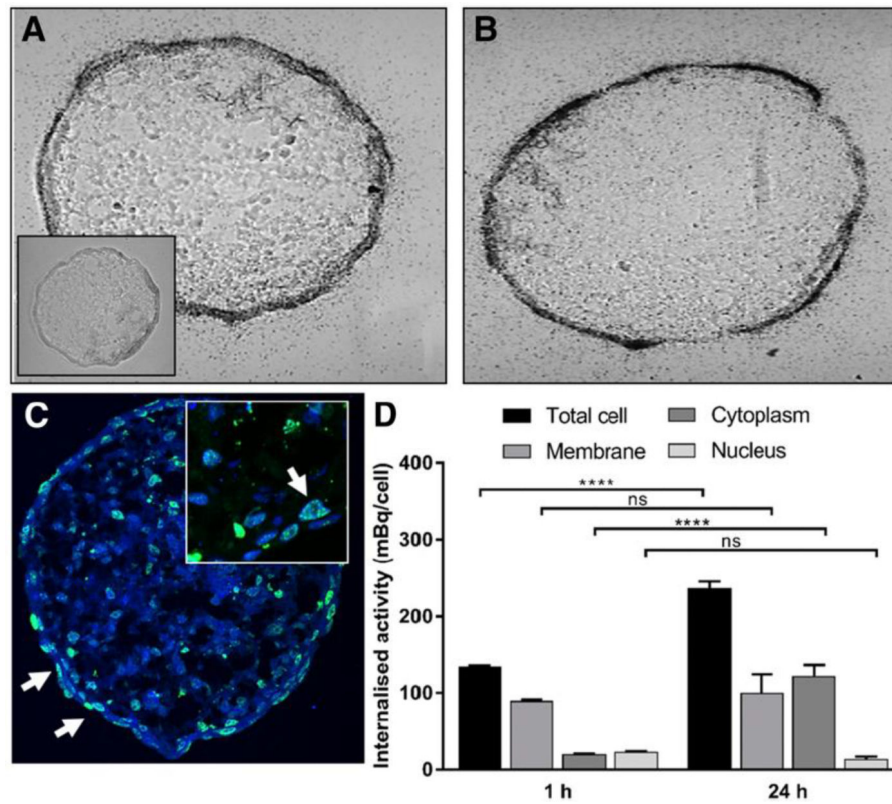
Figure 6.

Nonuniform activity distributions in multicellular spheroids affect tumor control probability. Spatial distribution of ^{111}In-EGF in SQ20B spheroids. Microautoradiograms of 8-μm spheroid sections after 1 h (inset shows control) (A) and 24 h (B) of treatment. (C) γH2AX expression in consecutive spheroid section after 24 h of treatment (inset shows peripheral distribution of foci within spheroid). (D) Internalized activity determined after 1 and 24 h of incubation. Figure adopted from Falzone et al. (Falzone et al. 2018).
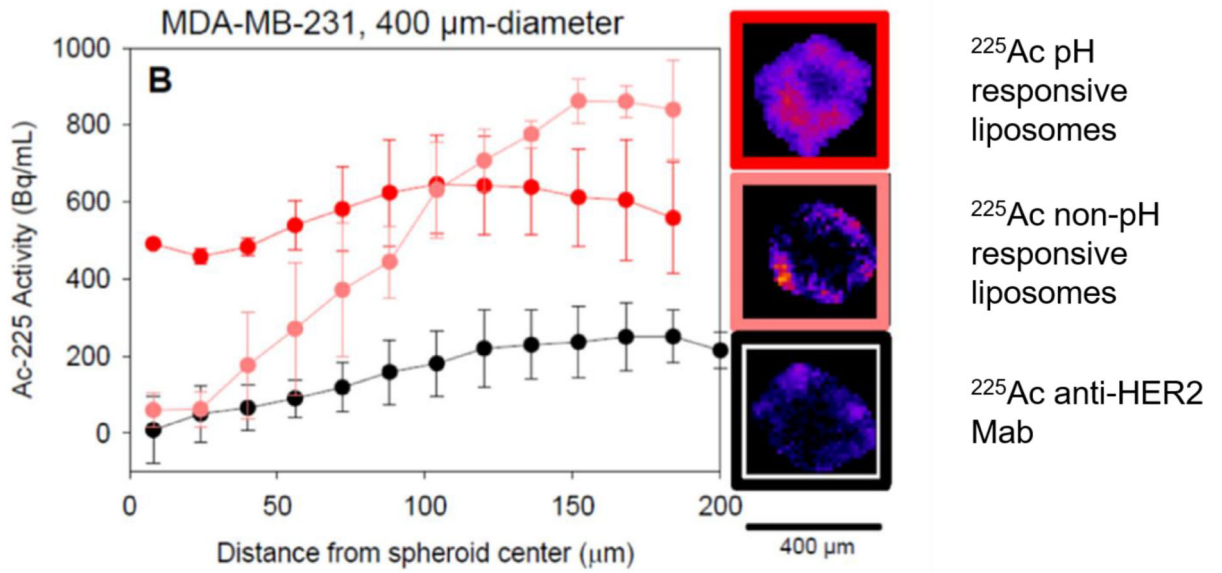
Figure 7.
pH sensitive liposomes can penetrate multicellular clusters to deliver radiopharmaceuticals more uniformly. Radial activity distributions and α-camera images of equatorial slices of MDA-MB-231-cell spheroids containing ^{225}Ac that was delivered by Ph-responsive liposomes, non-pH-responsive liposomes, and HER2-targeted radiolabeled antibody (Zhu C et al. 2017).
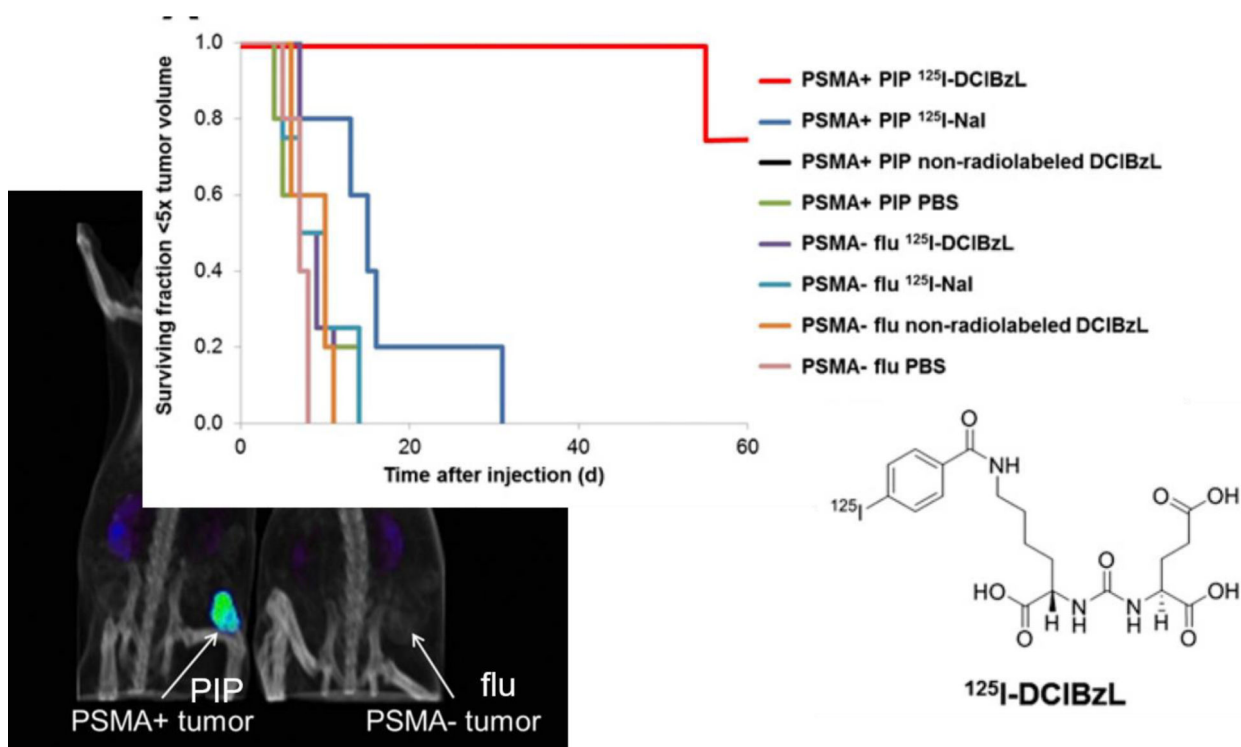
Figure 8.
Radiopharmaceutical therapy with a highly specific ^{125}I-labeled small molecule (DCIBzL) targeting the prostate-specific membrane antigen (PSMA). (*Lower right*) chemical structure of ^{125}I-DCIBzL. (*Upper*) Tumor growth delay in nude mice bearing PSMA$^+$ PC3 PIP or PSMA$^-$ PC3 flu flank xenografts after treatment with 111 MBq of ^{125}I-DCIBzL. (*Lower left*) SPECT/CT images obtained at 24 h after treatment with ^{125}I-DCIBzL. Tumor drug uptake is demonstrated in PSMA$^+$ PC3 PIP tumor but not in PSMA$^-$ PC3 flu tumor. Adopted from Kiess et al. (Kiess et al. 2015).

Functions of MNT modules

Selective binding and FR-mediated endocytosis due to FA

Endosome escape due to DTox
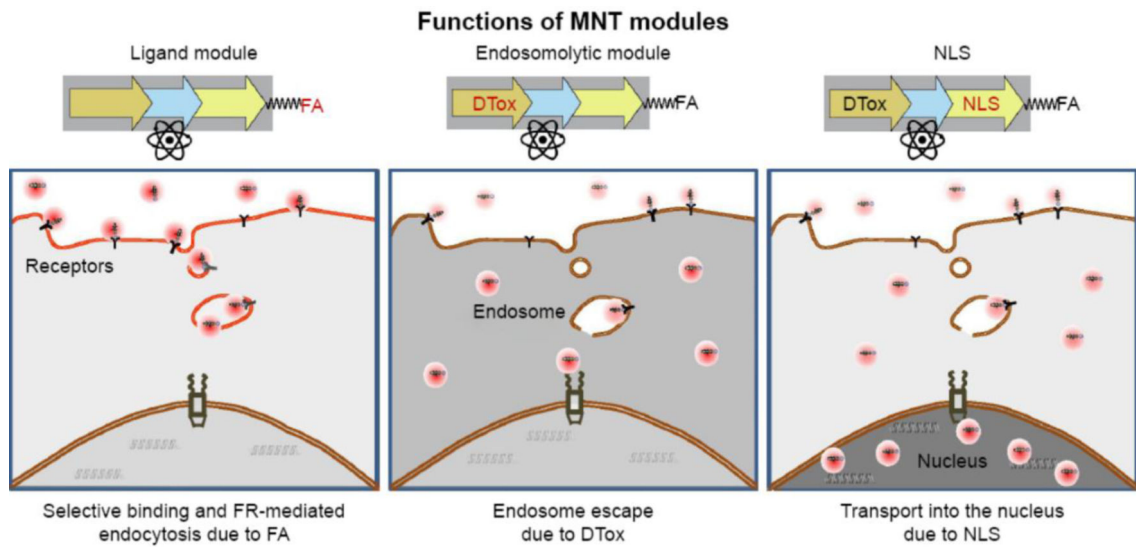
Transport into the nucleus due to NLS

Figure 9.

Modular nanotransporters (MNT, comprised of a ligand module, endosomolytic module, and nuclear localizing sequence) direct Auger electron emitters to folate-receptors (FR) on the cell surface and transport them into the cell nucleus (Slastnikova, Rosenkranz, Khramtsov, et al. 2017). (*Left*) selective binding of Auger-emitter-labeled ligand module to folate receptor and subsequent FR-mediated endocytosis due to folic acid (FA). (*Middle*) endosomolytic module uses diptheria toxin (DTox) to facilitate escape of MNT from endosome. (*Right*) the polyethylene glycol (PEG) nuclear localizing sequence module directs escaped MNT with Auger electron emitter into the cell nucleus. Adopted from (Slastnikova, Rosenkranz, Khramtsov, et al. 2017).